CHAPTER 6

RESULTS AND DISCUSSION - COAL PYROLYSIS

The analytical results for the char samples and the samples of gas liquor from the pyrolysis experiments are discussed in this section. As stated earlier in Chapter 3 of this thesis, the coal samples were heated to 600^{o}C at greater than 20bar for one hour under reducing conditions.

6.1 Chemical and mineralogical analyses of char samples

6.1.1 XRF analysis of char samples

The normalised XRF analyses of the char samples of coals taken from the six different mines (as produced in the pyrolysis experiments) are given in Table 6.1. The XRF analysis of coals from the six different coal mines was discussed in Chapter 4 of this thesis. The XRF technique used is semi-quantitative for sulphur, hence the sulphur contents are not reported in Table 6.1. Also, the results given in Table 6.1 reveal that there are significant variations in chemical compositions of the char samples produced. The significant differences between these chemical compositions are attributed to the coarse size of the coal samples ranging from 13.2mm to 2.36mm (and hence significant heterogeneity) in this study.

Table 6.1: XRF analyses of char samples obtained from the pyrolysis experiments

	Char-1	**Char-2**	**Char-3**	**Char-4**	**Char-5**	**Char-6**
Sample Number	*%*	*%*	*%*	*%*	*%*	*%*
SiO_2	57.90	56.94	55.80	51.86	53.23	53.40
Al_2O_3	26.50	30.01	27.90	29.30	27.80	24.82
Fe_2O_3	4.50	2.77	2.75	3.31	4.72	4.27
TiO_2	1.40	1.34	1.43	1.45	1.44	1.33
P_2O_5	0.40	1.13	1.12	1.55	1.54	1.83
CaO	6.10	5.24	7.94	9.11	8.10	10.89
MgO	1.10	1.03	1.43	1.35	1.33	1.83
Na_2O	0.60	0.62	0.71	0.73	0.72	0.92
K_2O	0.80	0.92	0.92	1.35	1.13	0.71

6.1.2 Mineralogical analysis of corresponding char samples

The mineralogical composition of corresponding chars tested in this study is given in Table 6.2. During the pyrolysis experiments, some minerals present in the coal partially transformed, with trends observed being in line with those summarised by Tomeczek and Palugniok (2002). Pyrite transformed to pyrrhotite. The kaolinite is expected to lose its bound water around 550^{o}C to form amorphous meta-kaolin. The high proportion of non-crystalline inorganic material in the char samples confirms the partial transformation of kaolinite to form meta-kaolinite during the pyrolysis experiments. Furthermore, the included minerals as well as the organically-bound inorganic elements could partially react with aluminium silicates (kaolinite and muscovite) at low temperatures under reducing conditions to form partially sintered particles. The XRD results for the char samples indicate that anhydrite formed during pyrolysis, probably from the interaction of the organic sulphur (and sulphur from the decomposition of pyrite) with organic calcium or with the included calcium-bearing fluxing elements-bearing minerals (calcite and dolomite).

In this study the thermodynamic package FactSage was used for undertaking the calculations, considering species in the gas phase, liquid phases and both solid compounds and solid solutions. It is clear from the results given in Table 6.3 that the FactSage model predicted the formation of high-temperature transformation products (anorthite ($CaAl_2Si_2O_8$), pyroxene (Mg, Fe)Si_2O_6, pyroxene ($CaMgSi_2O_6$)) of coal minerals (Table 3.4) at 600°C during coal pyrolysis under the reducing conditions. These calculated equilibrium phases that are generally observed only at temperatures of greater than 1000°C are not in good agreement with those of XRD. For example, Bryers (1986), Ward (1984) and Raask (1984) in their studies found that anorthite ($CaAl_2Si_2O_8$) formed when CaO reacted with reactive aluminium silicates such as metakaolin at high temperatures (1000-1200°C). The XRD analysis (Table 6.2) of the char samples from the pyrolysis experiments shows the presence of high proportions of coal minerals such as quartz and trace amounts of kaolinite, muscovite, dolomite, calcite and rutile as well as amorphous material in the char samples.

Table 6.2: Mineralogical composition of the corresponding char of coals mentioned in Table 4.5

Sample Number	Char-1 Mineral %	Char-2 Mineral %	Char-3 Mineral %	Char-4 Mineral %	Char-5 Mineral %	Char-6 Mineral %
Quartz	7.60	8.50	7.50	6.10	5.00	4.90
Kaolinite	1.70	2.50	1.60	0.80	1.30	1.20
Pyrite	0.00	0.00	0.00	0.00	0.00	0.00
Muscovite	1.30	2.00	1.20	1.30	1.20	-
Calcite	2.10	2.80	2.30	3.70	2.70	2.50
Dolomite	0.20	0.40	0.80	0.40	0.70	0.90
Pyrrhotite (Fe_7S_8)	1.40	0.80	0.60	0.60	0.60	0.50
Rutile	0.20	0.10	0.30	0.10	0.10	0.10
Anhydrite	0.20	0.60	0.30	0.30	0.30	0.30
Carbon and non-crystalline phases content	85.30	82.20	85.40	86.70	88.10	89.60

6.2 Pyrolysis results of the volatilised inorganic species

In this study, concentrations of inorganic elements in the gas liquor (determined by ICP-MS and IC) were used to calculate the amounts of inorganic elements vaporised during coal pyrolysis under conditions stated in Chapter 3. The IC analysis of all the gas liquor (pH values of 8.2 to 9.2) showed 800-1964ppm chloride, 64-91ppm bromide, 26-53ppm iodide, 0.01-0.04ppm fluoride, 800-1124ppm sulphate, 36-397ppm bicarbonate, 12 ppm carbonate, 6539-26000ppm ammonium, 28-40ppm sodium, 2ppm potassium, 0.2ppm magnesium, 6-14ppm boron, 5-7ppm calcium, 0.44-0.8ppm iron, 5.4-7.4ppm silicon, 0.2-1ppm aluminium and low concentrations of trace elements. The presence of these elements in the gas liquor clearly confirms volatilisation of these inorganic species during the pyrolysis of Highveld coal at a peak temperature of 600°C and pressure of 26bar. For all gas liquor samples analysed in this study, phosphate was not detected by IC, which implies that the volatilised trace phosphorus in the gas liquor is likely in the form of organic species.

Figures 6.1a to Figure 6.1g show the amounts of silicon, aluminium, iron, calcium, sodium, phosphorus and sulphur collected from the off-gas during pyrolysis. In these figures,

"distilled water" indicates the blank analysis, "200°C", "300°C", "400°C" and "600°C" the product of dissolution of gaseous products in distilled water for treatment up to the temperatures indicated, while "GL" is the condensed phase (water and organic liquid) for the whole pyrolysis treatment.

Of the coal samples tested, mine 5 coal followed by mine 6 coal released more volatile Si than all the other coals tested (Figure 6.1a); this was similar for Al and Fe (Figure 6.1b and c). Figure 6.1 gives the total amounts of the volatilised elements. These elements do not volatilise as inorganic species (based on the FactSage calculations and literature results) and must involve organic compounds.

Tar samples produced during the pyrolysis of the coal samples from the Highveld coal mines were analysed using FT-IR analysis to identify organometallic compounds in these samples. The FT-IR results for the tar samples revealed that these samples contain an aliphatic hydrocarbon, carboxylic acid, carboxylic acid salt, alcohol, epoxide, aromatic type of compound and metal carbonyls. Likely organometallic compounds in coal were summarised by Koppenaal and Manaham (1976) and include transition metal carbonyls, arene carbonyls, metal alkyls, organo hydrides and metal chelates. Recent results demonstrate that these compounds contribute to volatilisation: Zhang et al. (2006) showed (by X-ray photo-electron spectroscopy) that the sulphur, silicon, iron and sodium which are present in condensed volatile matter are organically bound. In addition, it was reported that the concentrations of silicon, aluminium and iron present in particulate matter (PM_1) particles (particles smaller than 1µm) after combustion in a drop-tube furnace were proportional to the amounts of these elements which are bound organically in the coal (Zhang et al., 2006).

The situation is different for the halogens in coals as given in Tables 6.3 and 6.4. The equilibrium calculations predict substantial volatilisation of chlorine (as HCl) and flourine (as HF); this is in line with the observation that as much as half of the chloride content of coal can be released as HCl, even at 300°C (Herod et al., 1983). In addition, some evaporation of NaCl may have occurred, since this has been shown to start at 597°C (Tomeczek and Palugniok, 2002), just below the peak temperature in these tests. In line with these predictions, the amounts of chlorine in the chars were significantly lower than in the coals (Table 6.3). The amounts of chlorine and fluorine in the coal and the corresponding char from the pyrolysis of mine 1 and mine 3 coals summarised in Table 6.4 were calculated by using

concentrations of chlorine and fluorine measured in these coals and the corresponding chars. In contrast with the FactSage (equilibrium) predictions, a smaller extent of volatilisation of fluorine than chlorine was observed during the pyrolysis of coal (Table 6.4). This could be attributed to the presence of fluorine as fluoroapatite in feed coal (Table 3.4), which decomposes at temperatures higher than 600°C.

Table 6.3: Predicted equilibrium compositions when 1.2kg coal with the composition as given in paragraph 3.4 equilibrates with 2.52mol N_2, at 600°C

Gas composition (major species and selected minor species shown); amount of gas is 21.5 mol

Species	Vol%
H_2O	30.98
CH_4	27.10
H_2	15.13
N_2	11.67
CO_2	10.23
H_2S	2.30
CO	1.85
HCl	0.60
NH_3	7.92E-02
HF	4.89E-02
COS	9.04E-03
HCN	6.59E-06
NaCl	5.23E-06
$FeCl_2$	4.41E-06
KCl	2.44E-06
$KFeCl_3$	2.26E-06
CS_2	2.02E-06
SiF_4	4.71E-08
$NaAlF_4$	1.55E-10
SiO	6.11E-23

Solids

Species	Mass (g)
Char (heated carbon)	566.4
Anorthite ($CaAl_2Si_2O_8$)	116.3
Quartz	59.1
Na feldspar ($NaAlSi_3O_8$)	33.8
Leucite ($KAlSi_2O_6$)	26.3
Pyroxene $(Mg,Fe)Si_2O_6$	21.4
Pyrrhotite	6.6
Pyroxene ($CaMgSi_2O_6$)	3.7
Hydroxyapatite $[Ca_5H(PO_4)_3]$	5.3
NaCl	2.3

Table 6.4: Amounts of halogens (Cl and F) in the 1200 g of coals and in 969 g of corresponding char from mine 1 and in 974 g of char from mine 3 before and after pyrolysis

Halogen	Mass of Cl and F in coal from Mine 1 (g)	Mass of Cl and F in char from coal Mine 1 (g)	Mass of Cl and F in coal from Mine 3 (g)	Mass of Cl and F in char from coal Mine 3 (g)
Cl	0.11	0.04	0.20	0.09
F	0.18	0.11	0.16	0.15

6.3 Calculated equilibrium volatilisation of cations in inorganic compounds from coal

The predicted equilibrium compositions of inorganic compounds are summarised in Table 6.3. As this shows, the dominant gaseous species are H_2O, CH_4, H_2, N_2, CO_2, H_2S, CO and HCl; the equilibrium vapour pressures of species containing Na, Fe, Al and K (chlorides), and Si (SiF_4 and SiO) are very low, with little removal of these elements predicted. In contrast, much of the fluorine and chlorine in the coal is removed to the gas phase, as HF and HCl. Of the 6g Cl in the coal, 4.6g is predicted to be removed by the gas phase, and all of the 0.2g F in the coal. This is in line with the chemical analyses of the char (as found experimentally), which indicate removal of the bulk of the halides by the gaseous pyrolysis products (Table 6.4). Similarly, of the 18.4g of S in the coal, 15.9g is predicted to be removed by the gas, partly as a result of decomposition of pyrite to pyrrhotite, but largely through the formation of volatile H_2S from the sulphur in the coal macerals. The predicted removal of Fe, Na, Si and Al is much smaller, at 80µg Fe, 26µg Na, 0.3µg Si, and approximately 1ng Al in comparison with the experimental results shown in Figure 6.1.

The low partial pressures of the species which contain Fe, Na, Si and Al are not unexpected. For example, the equilibrium constant of the reaction $SiO_2+4HF(g) = SiF_4(g)+2H_2O(g)$ is $K=(p_{SiF_4}\, p_{H_2O}{}^2)/(a_{SiO_2}\, p_{HF}{}^4)=30.9$ at 600°C. From the equilibrium gas composition, the partial pressure of HF is found to be 0.0125atm and that of H_2O 7.95atm. For equilibrium with pure SiO_2 that gives an equilibrium partial pressure of SiF_4 of 1.2×10^{-8}atm, which agrees with the volume percentage of SiF_4 as given in Table 4.39. Similarly, the formation of SiO would require a much higher temperature; at 600°C the equilibrium constant of the reaction $SiO_2+0.5C=SiO+0.5CO_2$ is $K= (p_{SiO}\, p_{CO_2}{}^{0.5})/(a_{SiO_2}\, a_C{}^{0.5})=2.5\times10^{-23}$, giving an equilibrium partial pressure of SiO of just 1.6×10^{-23} atm. Similar calculations for the Al- and Fe-bearing species support the predicted low equilibrium concentrations of volatile species of these elements in the pyrolysis product gas.

Note that volatilisation of all of these species is suppressed by increased oxygen levels in the inputs, since H_2O and CO_2 are co-products when respectively SiF_4 and SiO (as examples) are formed. Hence drying of the coal by removing the 3% water before the reactions occur, would favour greater volatilisation of Fe, Si and Al. However, this effect is quite small, since the major part of the hydrogen and oxygen in the off-gas originates from the coal macerals, not from the coal moisture.

To test this idea, the equilibrium for coal with no moisture and with the bound water removed from the kaolinite and muscovite before equilibration, was also calculated. For this case, the water vapour content of the product gas decreased to 26.4% and the CO_2 to 6.5%, and the HF content increased to 0.063%. The result though was only a slight increase in the SiF_4 content to 1.8×10^{-7}%, with 7.7×10^{-23}% of SiO - far too small to account for the observed volatilisation of silicon from the coal.

Based on these results, it does not appear possible for Fe, Na, Al and Si to be removed from the coal as volatile inorganic compounds during pyrolysis; this is in line with other results published in the literature (for example, Yan et al., 1999; Zhang et al., 2006). Yet the experimental results do indicate significant volatilisation of these elements. The only possibility appears to be that these elements are carried by volatile organic compounds. This suggestion is supported by the experimental observation that, in most cases, the largest part of the volatilised elements reports to the gas liquor (mixture of organic phase and aqueous phase), rather than being scrubbed out by the water scrubber.

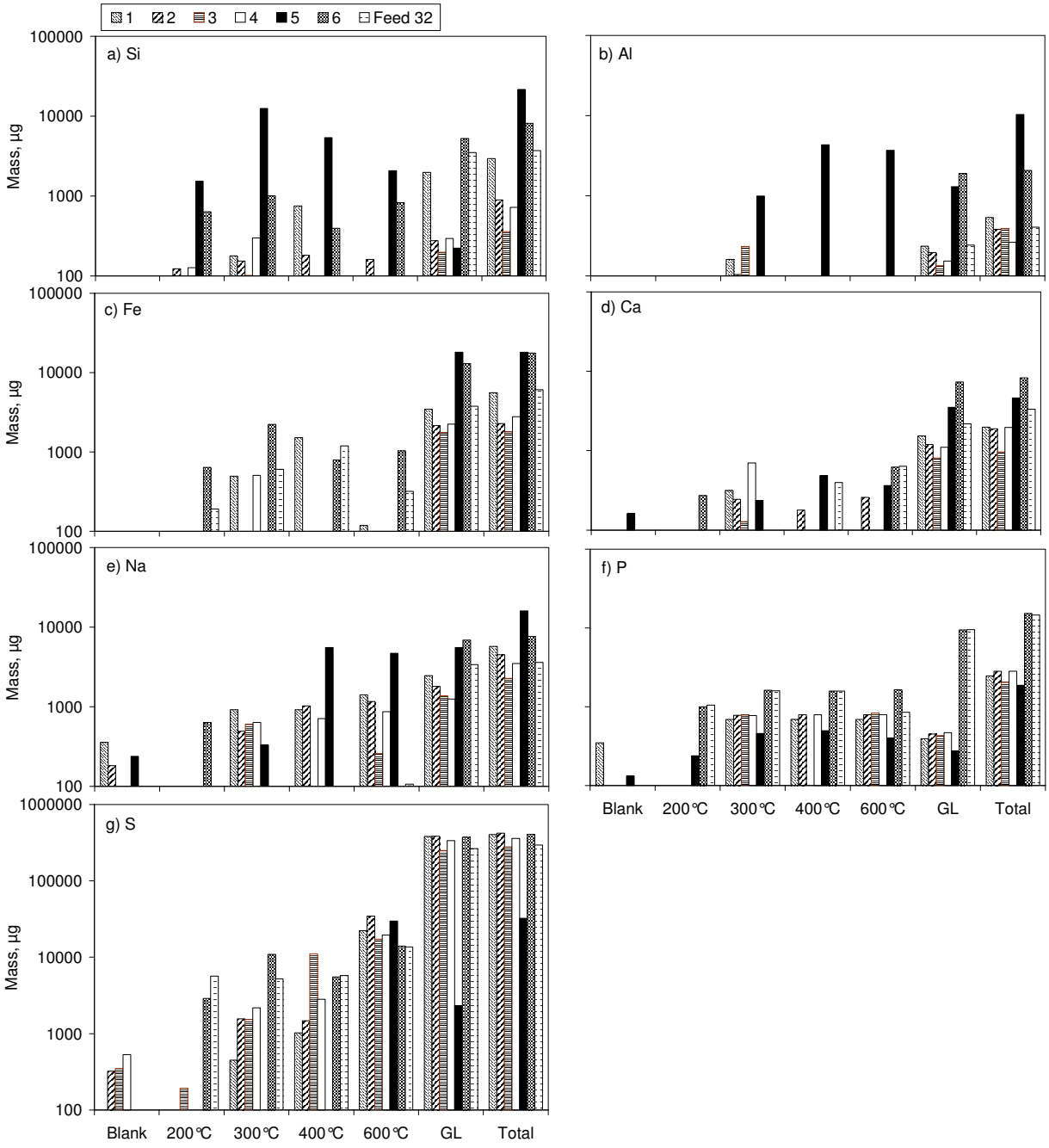

Figure 6.1. Amounts of elements volatilised during pyrolysis at various temperatures of various Highveld coal sources: a) Si; b) Al; c) Fe; d) Ca; e) Na; f) P; g) S.

CHAPTER 7

RESULTS AND DISCUSSION - GASIFICATION ASH ANALYSIS

The analytical results (chemical, physical and mineralogical analyses) for bulk gasification ash and gasification ash particles taken from the gasifier during gasifier test, turn-out and dig-out tests are discussed in this chapter. The main objective of this study was to determine inorganic components in the coal that are responsible for the clinker formation in the gasifier during coal gasification.

7.1 Chemical and mineralogical analyses of ash samples taken from the gasifier sampling methodology

7.1.1 Chemical analysis of corresponding ash samples

The chemical results for ash samples produced when using the experimental procedure described in Chapter 3 are summarised in Table 7.1. As noted earlier, a sample of corresponding gasification ash was collected from the bottom of the gasifier every three hours for an equivalent 24h period. At the end of the 24h period, the entire composite sample of coarse gasification ash was crushed and ground to obtain 100% passing 1mm. Before crushing the coarse ash fraction, clinker particles were hand-picked from this sample, based on their visual appearance.

The normalised ash elemental analysis values are reported in Table 7.1 and can be seen to be similar for the two sample types. A difference between the coarse ash and clinker is expected, as the clinker sample was hand-picked from the bulk gasification ash taken from the gasifier. The clinker was formed by physical contact between the heated rock fragment and the melt at elevated temperatures in the gasifier. The significant difference in concentrations of K, S and Ca in coal (Table 4.16) and ash samples could be attributed to significant volatilisation of these elements in the form of either sub-micron oxides ($CaO/CaSO_4$, K_2O) or gas (SO_2, H_2S).

The ultimate analysis (Figure 7.1) of the ash sample shows the expected low concentrations of S, H, N and C when compared with the coal sample. Trace amounts of sulphur in the coal ash can be captured by calcium oxide formed during transformation of either dolomite or calcite at elevated temperatures of greater than 1000°C to form calcium sulphate.

Table 7.1: Normalised XRF analysis of ash clinker and coarse ash samples and loss on ignition (L.O.I.) (wt%)

Sample Number	**Clinker**	**Coarse ash**
SiO_2	53.30	52.20
Al_2O_3	25.30	24.00
Fe_2O_3	5.30	4.90
TiO_2	1.40	1.30
P_2O_5	0.60	0.60
CaO	8.10	7.20
MgO	2.20	2.20
Na_2O	0.40	0.40
SO_3	0.50	0.50
K_2O	1.00	1.00
Total	100.00	100.00
L.O.I.	0.65	4.62

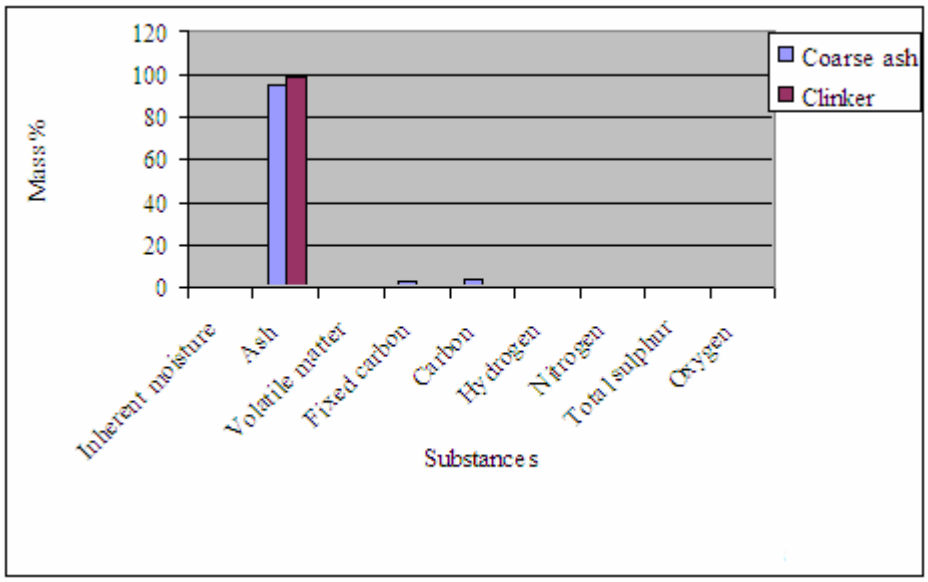

Figure 7.1: Ultimate and proximate analyses of ash particles.

7.1.2 Chemical composition of bulk gasification ash, heated stone and clinker samples from the turn-out test

Chemical analysis (Table 7.2) of samples from the gasifier turn-out indicates a wide variation in the composition of the individual ash, stone and clinker samples evaluated in the study. The main constituents in all cases are SiO_2, Al_2O_3, Fe_2O_3, CaO, MgO and TiO_2, with minor proportions (<1%) of Na_2O, K_2O, MnO, P_2O_5 and SO_3. Measurable concentrations of BaO and SrO occur in many of the coal gasification ash samples. The proportions of MgO, SrO and BaO can be correlated with the proportion of CaO (Figure 7.2), suggesting on the basis of other studies (Ward et al., 1999) that they are associated with the carbonate minerals in the feed coal.

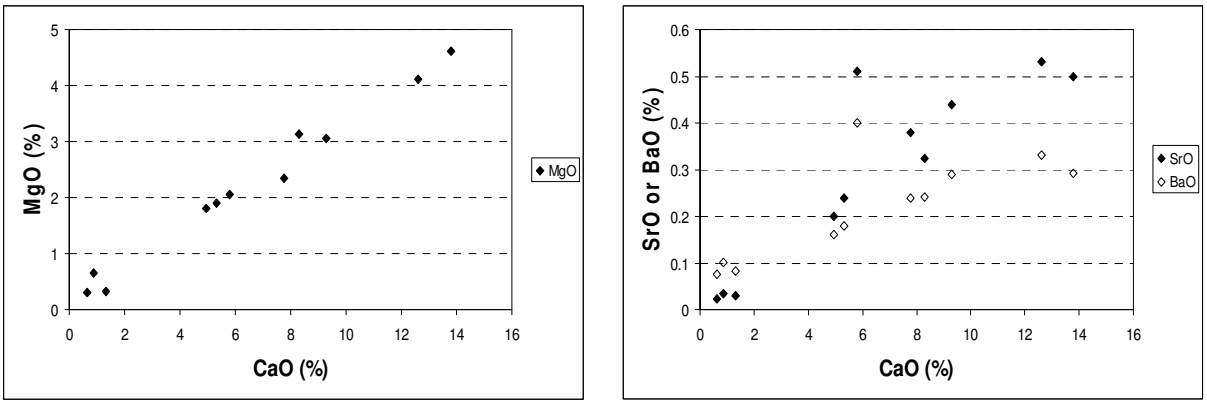

Figure 7.2: Correlation of MgO (left), SrO and BaO (right) with CaO in ash samples studied.

The composition of the bulk ash from the gasifier is similar to the ash chemistry expected from the mineral matter of the feed coal, calculated from the percentages and stoichiometric compositions of the minerals listed in Table 4.11. The abundance of bassanite has given rise to a greater percentage of (inferred) SO_3 in the LTA than that observed in the bulk gasification ash. The difference may reflect the higher temperatures associated with the gasification process, which would be expected to break down any calcium sulphates and convert more of the sulphur to the volatile form.

As discussed more fully below, the wide variations in chemical composition of the clinker samples are also reflected in the mineralogical composition of the materials, as well as the nature of the glasses occurring in the respective sample types.

Each sample typically represents an individual fragment of either coal or carbonaceous shale (stone) that occurred within the coarse feed coal, after being subjected to the high temperatures and pressures of the gasification process. For example, the results given in Table 7.2 indicate that the samples of partially burnt carbonaceous shale (heated stones 1 and 2) have higher concentrations of SiO_2 and K_2O and lower concentrations of Al_2O_3 and CaO than the clinker samples (1, 2, etc) analysed in the study. Based on data from a range of other South African coals and associated rocks (Pinetown et al., 2006), this suggests derivation from a material rich in quartz, feldspar and/or illitic clay minerals, rather than the kaolinite-rich clays and associated carbonate minerals (Table 7.2) associated with the coals themselves.

In most cases the white clinker particles (e.g. 4, 6) contain higher proportions of SiO_2 than the corresponding black or grey clinker particles (e.g. 3 and 5) and lower proportions of Fe_2O_3, CaO, SrO, MgO, K_2O, Na_2O and BaO (Table 7.2). The latter oxides, especially CaO, SrO, Na_2O, K_2O, MgO and Fe_2O_3 (which reacts as FeO), are generally thought to be associated with the sintering of coal ash materials. Briggs and Lindsay (Briggs, 1986) indicate that clay minerals may react with partially-oxidised pyrite and CaO from calcite at 750 -760°C to form silicate glass. Bryers (1986), Ward (1999) and Raask (1984) also indicate that CaO interacts with reactive aluminium silicates such as metakaolin at high temperatures (1000 -1200°C) to form gehlenite ($Ca_2Al_2SiO_7$) and anorthite ($CaAl_2Si_2O_8$), which in turn fuse at about 1400 to 1500°C.

Table 7.2: Chemical composition (wt %) of coal LTA inferred from XRD and of coal gasification ash, clinker and heated rock samples determined by XRF analysis

Oxide	Coal LTA	Bulk gasification ash	Clinker 1	Clinker 2	Clinker 3	Clinker 4	Clinker 5
SiO_2	54.30	49.40	41	48.7	49.8	60.9	49.30
Al_2O_3	28.20	24.40	24	27.9	25.8	23.4	23.70
Fe_2O_3	2.21	4.06	4.39	3.26	5.71	1.16	4.93
CaO	7.79	7.76	13.8	9.28	5.81	4.94	8.29
MgO	2.91	2.34	4.62	3.06	2.05	1.81	3.13
TiO_2	1.30	1.36	1.25	1.45	2.07	1.73	1.46
Na_2O	0.00	0.76	0.61	0.68	0.49	0.45	0.56
K_2O	0.60	0.88	0.67	0.72	1.01	0.54	0.69
MnO		0.05	0.075	0.06	0.05	0.08	0.06
P_2O_5	1.25	0.72	0.896	0.89	0.97	0.39	0.56
SO_3	1.44	0.25	0.221	0.102	0.03	0.09	0.68
SrO		0.38	0.498	0.44	0.51	0.20	0.32
BaO		0.24	0.293	0.29	0.4	0.16	0.24
ZrO_2		0.05	0.048	0.06	0.06	0.05	0.05
LOI		8.20	8.52	3.1	4.82	4.60	7.27
Total	100.00	101.00	100.01	100.00	99.70	101.00	101.00

Oxide	Clinker 6	Clinker 7	Clinker 8	Heated stone 1	Heated stone 2	Heated stone 3	Heated stone 4
SiO_2	61.00	56.50	43.2	76.90	80.01	52.50	57.40
Al_2O_3	28.80	26.50	27.7	9.89	10.70	25.30	25.80
Fe_2O_3	1.20	2.90	3.9	1.53	1.37	9.34	1.07
CaO	0.87	5.31	12.6	1.33	0.63	0.46	0.39
MgO	0.65	1.90	4.11	0.32	0.30	0.43	0.40
TiO_2	0.67	1.20	1.51	1.24	1.10	0.96	1.57
Na_2O	0.34	0.73	0.73	0.40	0.32	0.29	0.29
K_2O	1.25	1.32	0.68	2.19	2.44	1.72	0.90
MnO	0.01	0.04	0.08	0.02	0.01	0.011	0.00
P_2O_5	0.09	0.47	1.06	0.06	0.07	0.07	0.20
SO_3	0.00	0.05	0.04	0.19	0.23	0.29	0.21
SrO	0.03	0.24	0.53	0.03	0.02	0.02	0.11
BaO	0.10	0.18	0.33	0.08	0.08	0.08	0.16
ZrO_2	0.02	0.04	0.04	0.25	0.21	0.02	0.05
LOI	4.61	1.93	4.47	5.08	1.60	8.45	11.32
Total	99.70	99.10	101	99.70	99.20	99.90	99.90

Note: LOI = Loss on Ignition at 1050°C
Samples:
Coal LTA = inferred chemistry of coal ash based on mineralogy of LTA (Table 7.6)
Clinker 1 = A small heterogeneous clinker with black and white colours taken from the gasification ash exiting the gasifier.
Clinker 2 = A medium heterogeneous clinker with white and black colours taken from the gasification ash exiting the gasifier.
Clinker 3 = A large heterogeneous clinker with black colour taken from the gasification ash exiting the gasifier.
Clinker 4 = A large heterogeneous clinker with white colour taken from the gasification ash exiting the gasifier.
Clinker 5 = A largest heterogeneous clinker with black colour taken from the gasification ash exiting the gasifier.
Clinker 6 = A largest heterogeneous clinker with white colour taken from the gasification ash exiting the gasifier.
Clinker 7 = One lump of clinker sample taken from the bottom of the ash-bed area during turn-out sampling.
Clinker 8 = One lump of clinker sample taken from the gasification zone area during the turn-out sampling.
Clinker 9 = A large heterogeneous clinker with white and black colour taken from the gasification ash exiting the gasifier.
Clinker 10 = A largest heterogeneous clinker with white and black colour taken from the gasification ash exiting the gasifier.
Heated stone 1 = One lump of partially burnt carbonaceous shale taken from the gasification ash exiting the gasifier.
Heated stone 2 = One white lump of partially burnt carbonaceous shale taken from the gasification ash exiting the gasifier.
Heated stone 3 = One lump of partially burnt carbonaceous siltstone taken from the bottom of the ash-bed during turn-out sampling
Heated stone 4 = One lump of partially burnt carbonaceous sandstone taken from the gasification zone during turn-out sampling

7.2 Mineralogy of bulk gasification ash and clinker samples from the turn-out test

XRD analysis (Table 7.3) indicates that the bulk gasification ash sample contains around 10% quartz, together with 18% mullite ($Al_6Si_2O_{13}$), 13% anorthite ($CaAl_2Si_2O_8$) and around 50% amorphous glass. Small proportions of cristobalite (SiO_2) and diopside ($CaMgSi_2O_6$) are also present. The cristobalite was probably formed from the amorphous decomposition products of the clay minerals, kaolinite and illite. The remaining available amorphous silica may have reacted with high temperature transformation products (CaO and MgO) of carbonates (calcite and dolomite) to form diopside. The different clinker particles hand-picked from the gasification ash (clinkers 1, 2, 7, 8, 9 and 10) contain similar phases (including glass), although the proportions vary from fragment to fragment depending on factors such as composition and possibly the temperature reached by the fragment in the ash bed.

Samples of the partially burned carbonaceous shale taken from the gasification ash (heated stones 1 and 2), as well as partly burned siltstone and sandstone (heated stones 3 and 4), have higher proportions of quartz, but little (if any) anorthite, cristobalite or diopside. Table 7.3 indicates, for example, that heated stone 1 contains 7.9% illite, 6.4% pyrrhotite and traces of anatase and/or rutile (TiO_2), all of which presumably represent unaltered or partly altered remnants of the original sedimentary material. The presence of remnant illite particles in the heated stone samples is attributed to a combination of factors and processes, including incomplete thermal decomposition of the rock fragments entering the gasifier with the coal, the typical wide range of particle sizes (leading to incomplete fusion of the larger particles), and variations in operating procedures. The pyrrhotite (FeS) in heated stone 3 represents an alteration product of pyrite in the original rock, developed by heating under reducing conditions.

Dynamic high-temperature XRD studies on other materials (French et al., 2001) suggest that mullite and cristobalite form from the residues of clay minerals in the parent coal, especially the kaolinite, by solid state reactions that commence at around 1000°C. Solid-state reactions in calcium-rich mineral matter produce anorthite at similar temperatures, with quartz and/or clay mineral residues being incorporated into the anorthite as part of the process.

When tested at progressively higher temperatures the anorthite begins to react with the melt at around 1200°C, while the mullite and cristobalite in Ca-poor ashes begin to react with the melt at around 1400°C. Cooling of the molten material, especially the slow cooling associated with the gasifier bed, may also be expected to produce crystals of anorthite, as well as the pyroxene mineral diopside, in a manner analogous to the crystallisation of magmas in igneous rock formation.

Table 7.3: Mineralogy of coal gasification ash, clinker and heated rock samples by XRD and Siroquant (wt %)

Mineral	**Bulk coal gasification ash**	**Clinker 1**	**Clinker 2**	**Clinker 3**	**Clinker 4**	**Clinker 5**	**Clinker 6**
Quartz	10.7	3.9	0.2	3.7	10.6	5.5	14.6
Anorthite	13.1	27.0	51.6	19.5	10.4	38.8	2.3
Mullite	17.7	5.7	9.5	13.9	22.1	10.7	29.7
Cristobalite	1.8		1.7	5.5	10.2	4.2	
Diopside	0.7	12.1		1.9	0.9		
Illite							
Anatase							
Rutile							
Calcite							
Dolomite							
Pyrrhotite							
Amorphous*	56.0	51.3	37.0	55.7	45.8	40.8	53.4

Mineral	**Clinker 7**	**Clinker 8**	**Heated stone 1**	**Heated stone 2**	**Heated stone 3**	**Heated stone 4**
Quartz	12.9	1.5	61.8	50.8	21.3	24.9
Anorthite	8.4	62.3	3.2	2.3		
Mullite	17.0	5.8	14.8	7.7	19.7	
Cristobalite		1.0				
Diopside		12.1				
Illite					7.9	
Anatase	0.1				0.6	1.1
Rutile						0.8
Calcite						
Dolomite						0.3
Pyrrhotite					6.4	
Amorphous*	61.6	17.3	20.1	39.2	44.2	73.0

Note: * Includes both non-crystalline glass and any unburnt carbon (char) components

7.2.1 Interpretation of glass composition from XRD and chemical data

Tables 7.4 and 7.5 provide data on the inferred chemical composition of the crystalline minerals and the glass phases in the ash, clinker and heated rock (stone) samples, estimated from the XRD and whole-sample chemical data (Tables 4.11 and 7.2), following the

methodology described by Ward and French (2006). As might be expected from the nature of the materials, a wide range of compositions is implied by these results, especially for the glassy phases. For some samples, such as clinker 1 and heated stone 2, the crystalline and glassy components appear to have similar overall compositions, at least with respect to the major oxides (SiO_2, Al_2O_3 and CaO). For most others, however, such as the bulk gasification ash, heated stone 1 and clinkers 2-6, the glass fraction appears to have a higher proportion of SiO_2 and a lesser proportion of Al_2O_3. The partitioning of CaO within this group varies, although most samples appear to have similar to higher proportions of CaO in the crystalline phases compared to the glassy components. MgO is mostly present in the glass phase only.

Negative percentage values are noted in some instances. These may reflect over-estimation of the abundance of particular crystalline phases (e.g. anorthite), or possibly under-estimation of glass content, by the XRD technique.

As pointed out by Ward and French (2006), the material identified as glass by the XRD technique is not necessarily of uniform composition within the individual ash samples. It may also include particles of crystalline components that are too low in abundance or too small in particle size to be identified separately by X-ray diffraction methods. Some of the crystalline phases, such as mullite, may also have different chemical compositions to the stoichiometric data used in interpreting the XRD results. Although the electron microprobe study has identified some discrete solid particles made up mainly of Fe and Ti (see below), these make up only a small proportion of the relevant ash or slag samples. None of the crystalline phases identified in the samples by XRD techniques would normally be expected to contain iron, titanium, magnesium or sodium; these elements are therefore interpreted from the XRD and bulk chemical data to occur only in the glassy phases of the samples studied.

Table 7.4: Inferred composition (wt%) of mineral and glass fractions for gasification ash and clinker samples

Sample	**Bulk gasification ash**		**Clinker 1**		**Clinker 2**	
	Minerals	**Glass**	**Minerals**	**Glass**	**Minerals**	**Glass**
Fraction	*44.6*	*55.4*	*48.7*	*51.3*	*63*	*37*
SiO_2	53.43	53.98	49.66	40.25	43.55	62.89
TiO_2	0.67	2.13		2.66		4.08
Al_2O_3	38.87	16.62	28.14	24.44	39.99	10.43
Fe_2O_3		7.97		9.36		9.17
MgO		4.59	4.62	5.46		8.61
CaO	6.5	10.01	17.58	12.73	16.46	-1.92
Na_2O		1.49		1.3		1.91
K_2O		1.73		1.43		2.03
P_2O_5		1.41		1.91		2.5
SO_3	0.53	0.07		0.47		0.29
Total	100	100	100	100	100	100

Sample	**Clinker 3**		**Clinker 4**		**Clinker 5**	
	Minerals	**Glass**	**Minerals**	**Glass**	**Minerals**	**Glass**
Fraction	*44.5*	*55.5*	*54.2*	*45.8*	*59.2*	*40.8*
SiO_2	51.26	54.62	59.3	69.19	50.52	56.22
TiO_2		3.98		3.96		3.84
Al_2O_3	38.03	19.1	36.11	10.82	36.31	9.58
Fe_2O_3		10.98		2.65		12.95
MgO	0.79	3.3	0.31	3.78		8.22
CaO	9.91	3.22	4.29	6.23	13.17	2.66
Na_2O		0.94		1.03		1.47
K_2O		1.94		1.24		1.81
P_2O_5		1.86		0.89		1.47
SO_3		0.06		0.21		1.78
Total	100	100	100	100	100	100

Sample	**Clinker 6**		**Clinker 7**		**Clinker 8**	
	Minerals	**Glass**	**Minerals**	**Glass**	**Minerals**	**Glass**
Fraction	*46.6*	*53.4*	*38.4*	*61.6*	*82.7*	*17.3*
SiO_2	51.49	75.47	55.77	59.91	46.49	39.14
TiO_2		1.32	0.26	1.85		9.14
Al_2O_3	47.52	15.38	39.57	19.73	31.85	15.33
Fe_2O_3		2.37		4.86		23.6
MgO		1.28		3.18	2.72	11.86
CaO	0.99	0.85	4.4	6.16	18.93	-14.26
Na_2O		0.67		1.22		4.42
K_2O		2.47		2.21		4.11
P_2O_5		0.18		0.79		6.41
SO_3				0.09		0.24
Total	100	100	100	100	100	100

Table 7.5: Inferred composition (wt%)of mineral and glass fractions for heated stone samples

Sample	Heated stone 1		Heated stone 2		Heated stone 3		Heated stone 4	
	Minerals	Glass	Minerals	Glass	Minerals	Glass	Minerals	Glass
Fraction	*79.8*	*20.2*	*60.8*	*39.2*	*55.8*	*44.2*	*27*	*73*
SiO_2	84.45	71.16	88.8	72.34	55.2	60.3	92.2	55
TiO_2		6.53		2.89	1.1	1	6.7	0
Al_2O_3	14.74	-6.19	10.44	11.9	30.5	24.2		40.1
Fe_2O_3		8.05		3.6	5.3	16.5		1.7
MgO		1.68		0.79		1.1	0.2	0.5
CaO	0.81	3.82	0.76	0.47		1.1	0.3	0.5
Na_2O		2.11		0.84		0.7		0.5
K_2O		11.53		6.41	1.3	2.6		1.4
P_2O_5		0.33		0.17		0.2		0.3
H_2O					0.7	-0.8		
CO_2							0.5	-0.2
S					6	-7.6		
SO_3		0.98		0.6		0.7		0.3
Total	100	100	100	100	100	100	100	100

7.2.2 XRD analysis of the homogenised selected dig-out samples

From Appendix D, Table D1 it is clear that kaolinite, illite and dolomite decreases from sample 1D (top of the gasifier) to sample 11D. This implies that as the temperature of the gasifier increases, minerals in the coal transform to form high temperature transformation products. The presence of mullite, cristobalite, anorthite and diopside ($CaMgSi_2O_6$) in some of the ash samples indicate that these minerals were derived from the mineral transformation at elevated temperatures and pressures during gasification, since these minerals were not present in the feed coal to generate the ash.

XRD analysis also indicates that the proportion of mullite increases from samples 6D-11D. Kaolinite transforms at elevated temperatures of greater than 800°C to form reactive aluminosilicate (metakaolinite) and amorphous quartz (Grim, 1962; Bryers, 1986; Unsworth et al., 1987b; Ward and French, 2004; van Alphen, 2005). As the temperatures of the ash particles increase further to greater than 1000°C, some metakaolinite and amorphous quartz particles further transform to form mullite and cristobalite respectively. Some other amorphous quartz particles react with high temperature transformation products (CaO and MgO) of carbonates (dolomite and calcite) to form diopside. Some reactive metakaolinite can react with either CaO or MgO to form a melt.

On cooling the ash with steam injection at the bottom of the gasifier, anorthite and to a lesser extent mullite begins to crystallise out from the melt (Matjie et al., 2006). The presence of anorthite and mullite in the dig-out samples 6D-11D indicates the interaction of kaolinite and dolomite at high temperatures resulting in a melt formation and anorthite and mullite subsequently being crystallised out from the melt.

As indicated previously, quartz grains which might otherwise react to form feldspar or glass, can also persist as essentially unreacted particles throughout the different stages of the gasification process (Matjie et al., 2008). The XRD results for all of the dig-out samples (showing a significant proportion of quartz) confirmed the previous results.

7.2.3 XRD analysis of the homogenised turn-out samples

The XRD analysis of the turn-out samples taken from the gasifier is summarised in Appendix C, Tables C1and C2. The concentrations of minerals and non-crystalline phases in these samples added up to 100%. The data for these samples indicate the following trends:

- Sample 32T, which is the feedstock for the gasification process, contains mainly kaolinite (6,7%), quartz (6.0%) and dolomite (2%) with minor proportions of muscovite (1.1%), calcite (1.2%), aroganite (1.2%), pyrite (0.4%), rutile (0.3%), greigite (0.2%), gorceixite ($BaAl_3(PO_4)PO_3OH)(OH)_6$) (0.2%). Such mineral assemblage is consistent with similar results for the LTA of the same feed coal presented in Tables 4.11 and 7.3.
- As expected, the total non-crystalline content (80%) of carbon in sample 32 was found to be the highest when compared to the carbon content of other turn-out samples that were exposed to elevated temperatures.
- Dolomite was found to be present in samples 24T and 32T that were taken from the top of the gasifier. In samples from lower in the gasifier, the dolomite had completely transformed to form either magnesium oxide or calcium oxide. These oxides preferentially react with the transformed product of kaolinite to form a melt. Some CaO and MgO reacted with reactive silica from the transformation of kaolinite to form diopside ($CaMgSi_2O_6$). The absence of dolomite and aragonite and a low proportion of kaolinite in sample 16T (heated to 1000°C), could imply that magnesium and calcium

from the transformed dolomite initially reacts with the transformed kaolinite (metakaolinite) to form a melt under reducing and oxidising conditions during coal gasification.

- Calcite persisted at elevated temperatures and is still contained in sample 8T, which was taken from the bottom of the ash-bed in the gasifier. According to Bryers (1986), Ward (1984) and Raask (1984), CaO from calcite reacted with reactive aluminium silicates such as metakaolin at high temperatures (1000-1200°C) to form anorthite ($CaAl_2Si_2O_8$), which in turn fused at about 1400-1500°C. This could imply that some calcite transformed at elevated temperature of greater than 1000°C to form CaO, which preferentially reacted with reactive alumino-silicate to form anorthite under oxidising conditions. The presence of anhydrite, which is a product of calcium oxide and sulphur dioxide, was found to in samples 1T, 8T and 16T.
- According to XRD analysis of the turn-out samples, pyrite transformed to pyrrhotite, magnetite and hematite and contributed minimally to the sintering or slagging mineral matter during coal gasification.
- Kaolinite was found to be present in samples 32T, 24T and 16T and started to transform at elevated temperatures (sample 16T) and completely transformed to a reactive alumino-silicate (metakaolinite) in samples 1T and 8T.
- Interestingly the concentration of quartz in the turn-out samples does not vary significantly. These results confirm that quartz can persist as unreacted particles throughout the different stages of the gasification process.

7.2.4 QEMSCAN images of the clinker samples

QEMSCAN images of the clinker samples taken from the turn-out samples are illustrated in Appendix Figure C1. The pink and green areas that are shown in these images are unreacted quartz and dehydrated kaolinite present in the crystalline phase (anorthite) and glass matrix.

The bottom image of the clinker sample 8T clearly shows heated laminated siltstone/mudstone fragments on the left with pink quartz and green /blue clay (Figure C1). From the top right of the bottom image, the fragment of feldspathic sandstone set in a feldspar rich matrix. The glass to centre left (red) of the bottom image is of a different chemical composition.

These QEMSCAN results revealed that the heated siltstone/mudstone and sandstone rock fragments physically attached to the feldspar-rich matrix, without reacting with the melt during coal gasification. The CCSEM results given in Figures 7.3 and 7.4 are in good agreement with the QEMSCAN results.

7.2.5 CCSEM of coarse ash and clinker mineralogy

Macroscopically, the coarse ash mainly consists of rock fragments ("stone") in a black matrix (Figure 7.3). The black matrix has distinct elongated crystalline laths (dark grey) in the Ca/CaMg/Fe-bearing aluminosilicate glass (light grey) matrix (Figure 7.4). Based on the elemental proportions, these crystalline laths are anorthite ($CaAl_2Si_2O_8$) and the glass is principally the Ca/CaMg/Fe-bearing aluminosilicate glass with varying proportions of Ca, K, Ti, Fe, P and Mg. The anorthite crystals are presumed to have crystallised from the melt during cooling.

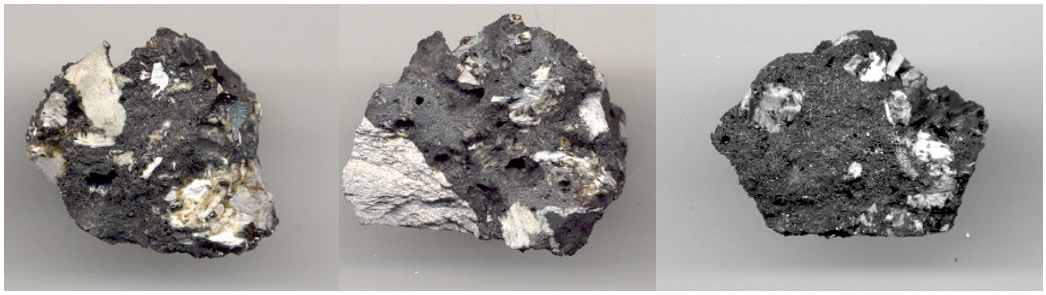

Figure 7.3: Hand-picked clinker fragments: "Stone" fragments (light colour) in black "glass" matrix.

The quartz (Q) grains in the quartz-kaolinite-muscovite-microcline siltstone fragment (Figure 7.4) have defined grain boundaries. The "honeycomb" structures (Ka) were originally kaolinite, which dehydrated (leaving the observed cavities). The light grey interstitial phase is K-bearing aluminosilicate derived from muscovite/illite. Rising steam and the cessation of carbon gasification lowers the temperature and initiates crystallisation of anorthite and to a lesser extent mullite from the melt. As the ash-bed subsides towards the rotating grate, the temperature decreases further and the residual molten material solidifies into a Ca- and Fe-bearing aluminosilicate glass. The interstitial glass is a Ca- and Fe-bearing aluminosilicate with varying proportions of K, Ti, P and Mg.

Simplistically, the Ca/CaMg/Fe-bearing aluminosilicate glass can be classified into four broad types, depending on the proportion of Ca/Mg and Fe. These are:

- Ca-aluminosilicate glass - Ca/Mg content is variable, with trace concentrations of Fe; K and Ti can occur.
- Ca-Fe-aluminosilicate glass - Ca/Mg and Fe content are variable; trace concentrations of K and Ti can occur.
- Fe-aluminosilicate glass - Fe content is variable; trace concentrations of Ca, K, Mg and Ti can occur.
- Silica-rich glass with minor and varying concentrations of Al, Ca, K, Mg, Fe and Ti.

The proportion of Ca/CaMg/Fe-bearing aluminosilicate glass relative to anorthite is extremely variable. On a microscopic scale, anorthite tends to occur in isolated clusters separated by the Ca/CaMg/Fe-bearing aluminosilicate glass devoid of anorthite laths and rock fragments. In addition to anorthite, mullite ($Al_6Si_2O_{13}$) needles in the glass were also identified. These mullite needles are extremely fine and are not common (Figure 7.4).

Minor coarse Fe-oxide/Fe-S-oxide rich, Ca-oxide/CaMg-oxide-rich and carbon-rich particles were identified in the pulverised bulk gasification ash. The Fe-oxide/Fe-S-oxide rich particles and Ca-oxide/CaMg-oxide either occur as extraneous particles or are attached to Ca/CaMg/Fe-bearing aluminosilicate glass.

The Fe-oxide/Fe-S-oxide particles comprise pyrrhotite, Fe-S-oxide and Fe-oxide and represent the transformed products of pyrite (Srinivasachar et al., 1990a; 1990b; Matjie et al., 2006; Bryers, 1986). This mineral originally occurred as coarse pyrite-rich cleat fillings in the coal (Figure 4.3). As the CCSEM cannot distinguish between hematite (Fe_2O_3), magnetite (Fe_3O_4) and wustite (FeO), these phases are grouped as “Fe-oxide”.

The Ca-oxide and CaMg-oxide rich particles are grouped as “Ca-Oxide/CaMg-oxide”. It is concluded that these Ca-oxide/CaMg-oxide particles are transformed coarse calcite/dolomite cleat fillings originally present in the coal (Deer et al., 1992; van Alphen, 2005; Briggs, 1986; Bryers, 1986).

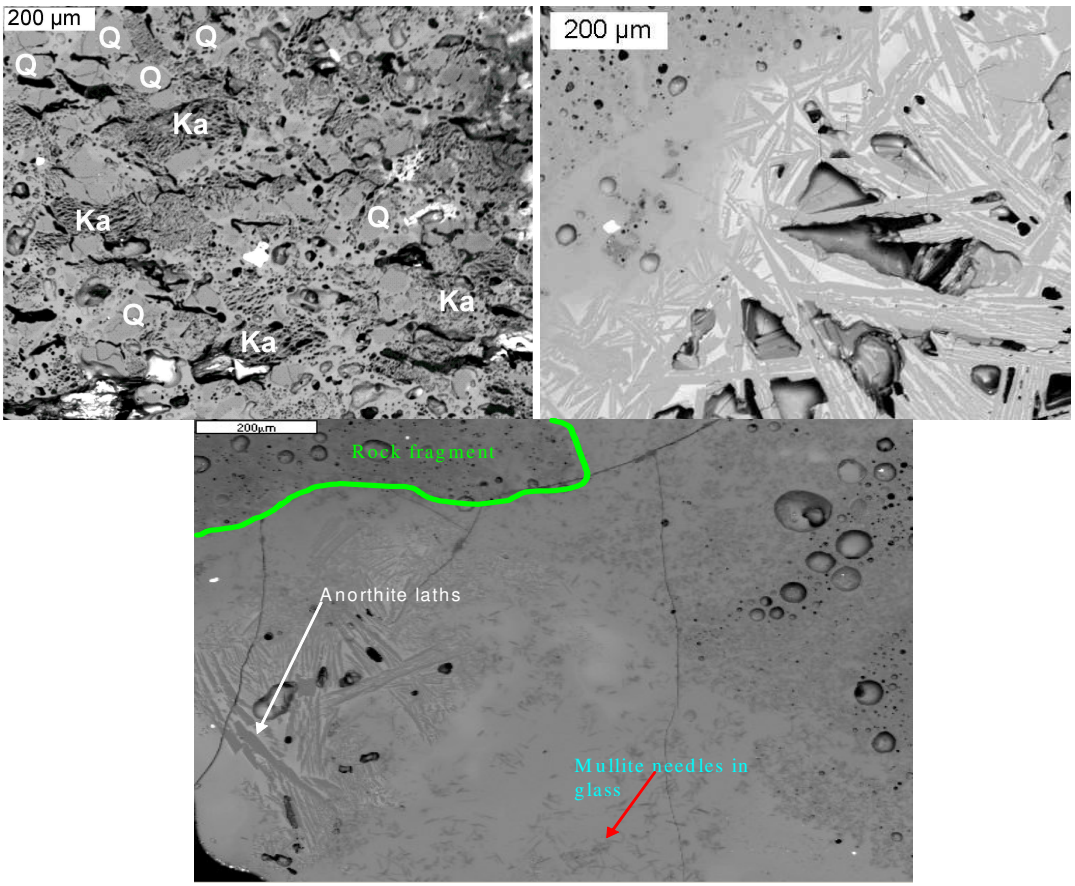

Figure 7.4: Detail of rock fragment (left image) and grey elongated anorthite crystals and Ca- and Fe-bearing glass matrix (light grey). The bottom image shows crystallisation of anorthite and mullite from a melt and physical contact between rock fragment and the melt.

7.2.6 Phase proportions in coarse ash and clinker fragments

The mass percentages of phases in the coarse ash and clinker sample (as measured by CCSEM) are summarised in Appendix B, Table B1. XRD results of the coarse ash and clinkers indicated that the major crystalline phases are: anorthite (27.7%), quartz (37.7%) and mullite (26.6%) in the coarse ash; and anorthite (52%), mullite (23.8%) and quartz (22.3%) in the clinker sample. Minor albite (6.8%), augite (2.5%), hematite (2%) and magnetite (0.3%) are present in the coarse ash; and augite (2%) and hematite (0.2%) in the clinker. Glass phases were not analysed by XRD. The XRF analysis of ash samples (coarse ash and clinker) indicated that these samples contain 52.2% SiO_2, 24.0% Al_2O_3, 5.3% Fe_2O_3, 1.3% TiO_2, 0.6% P_2O_5, 7.2% CaO, 2.2% MgO, 0.4% Na_2O, 1.0%K_2O and 0.5% S (normalised XRF results).

7.2.7 CCSEM analysis of hand-picked coal and clinker particles

Simplistically, the coal feedstock consists of organic-rich coal particles with varying proportions of included minerals, mineral rich rock fragments or "stone" derived from floor, hanging wall and in-seam partings and coarse pyrite-rich and calcite-rich cleat fragments.

CCSEM and XRD analyses (Table 4.3, Table 4.5, Table 4.12 and Figure 4.3) of the coal feedstock to the gasification process indicate that this coal contains major minerals (kaolinite, quartz and dolomite) and minor minerals (pyrite, calcite, muscovite/illite, apatite, microcline and rutile). The grains of kaolinite and quartz occur in organic-rich coal particles and significant proportions of these minerals occur in siltstone, mudstone and sandstone rock fragments (Figure 4.3). In most cases calcite and pyrite mainly occur in cleats in organic-rich coal particles (Figure 4.3). Dolomite is associated with calcite-rich cleats. The K-bearing microcline and muscovite/illite are mainly associated with kaolinite and quartz in the siltstone and mudstone rock fragments (Figure 4.3).

Macroscopically, the coarse ash and clinkers consist of rock fragments ("stone") in a matrix of "glass" (Figure 7.4). The included fluxing elements-bearing minerals such as pyrite, dolomite and calcite react with the included kaolinite to form a melt. On cooling a melt with steam during the coal gasification process, the crystalline phases such as anorthite and to a lesser extent mullite, crystallised out from the melt and amorphous phase (glass) is formed. Some heated rock fragments from the surroundings attach to the melt to form heterogeneous clinkers. The chemical and mineralogical composition of the heated rock fragments in a clinker sample is controlled by the interaction of mineral matter present in the original coal sample.

It was visually observed that the hand-picked clinkers analysed in this study have distinct vesicles or voids with a reddish brown surface. It is proposed that these vesicles are the frozen remnants of steam or air bubbles that passed through the molten clinker. On cooling of the clinkers, the partially oxidised iron or ferrous in the glass further reacted with steam or air to form ferric hydroxides. This produced the "rust" surface colour of the bubbles.

It is clear from Figure 7.5 that randomly-orientated elongated anorthite laths crystallised out from the melt during cooling. The Ca-, Fe-, Mg-bearing aluminosilicate glass with varying

chemical composition was formed. The proportion of glass to anorthite can vary significantly and is localised. Although, not as common as anorthite, thin mullite needles and spinel are present (Figure 7.5). The formation of anorthite through crystallisation implies that dolomite and calcite reacted with aluminium silicate (kaolinite) at elevated temperatures to form a melt. On cooling anorthite crystallised out from the melt. The presence of anorthite and mullite crystals in these clinkers was confirmed by the electron microprobe and CCSEM analyses (Figure 7.5, Figure 7.4 and Figure 7.17). Anorthite laths and Fe- and Mg-bearing aluminosilicates were identified in sample 1T, sample 8T and sample 16T. These samples are below the gasification zone and have been exposed to temperatures exceeding 1000°C.

Fine mullite and corundum needles in glass were identified in sample 1T only (Figure 7.5). These mullite crystals can occur with anorthite (Figure 7.5) or as the only crystalline phase in the glass. Unlike anorthite, the proportion of mullite relative to glass is comparatively low and the mullite needles are smaller than anorthite. The mullite rich areas were in close proximity to remnant rock fragments. The mullite needles in sample 8T (identified by CCSEM) are derived from the reaction of kaolinite and pyrite or dolomite at elevated temperatures. A high ratio of alumina to silica in the melt could enhance the formation of a significant amount of mullite crystals.

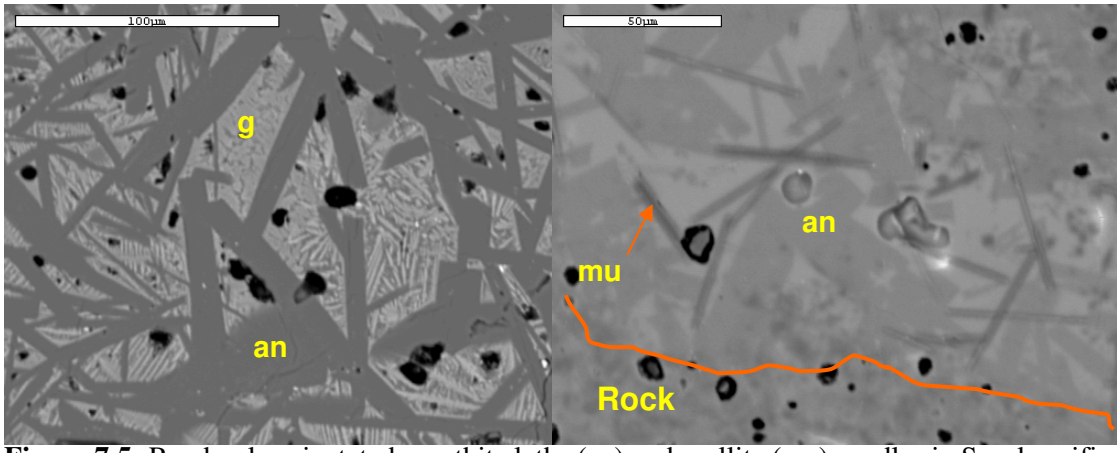

Figure 7.5: Randomly orientated anorthite laths (an) and mullite (mu) needles in Sasol gasification ash. Image on left is from sample 8T and on the right sample 1T. Glass is light grey (g). Note the glass in sample 8T is differentiated into two phases, whereas sample 1T interstitial glass is uniform. Scale bars represent 100µm and 50µm, respectively.

The interstitial glass is enriched in Fe (some iron particles are derived from kaolinite/pyrite association, siderite and ankerite) and to a lesser extent Mg relative to the average field composition. This trend is expected as Fe and Mg cannot be accommodated into the anorthite structure. On further cooling, the Fe and Mg in the interstitial glass reacts with aluminosilicate or oxygen to form the following iron species, Fe-rich Mg-aluminosilicate (pyroxene or amphibole), Fe-rich hercynite ($FeAl_2O_4$) and finally wustite. The Mg reacts with aluminosilicate and alumina to form MgFe-aluminosilicate and Mg-rich spinel ($MgAl_2O_4$) respectively (Figure 7.6). The excess Al will partition into mullite, Mg-rich spinel and corundum (Al_2O_3). The Fe-Mg silicate minerals in the analysed clinkers may have been derived from reactions between fluxing elements-bearing minerals (pyrite, calcite and dolomite) and kaolinite or illite at elevated temperatures during coal gasification. During the transformation of pyrite, which is associated with organic-rich particles in the coal, iron can be formed. The iron may react with inorganic elements or substances to form a spinel such as magnesioferrite ($MgFe_2O_4$), which dissolves in the melt formed from the decomposition products of kaolinite, calcite and pyrite at 750-760°C to form Fe-Mg silicate glass (Briggs, 1986). The increase in Fe and partitioning of the interstitial glass into different Fe-bearing phases is illustrated in Figure 7.6.

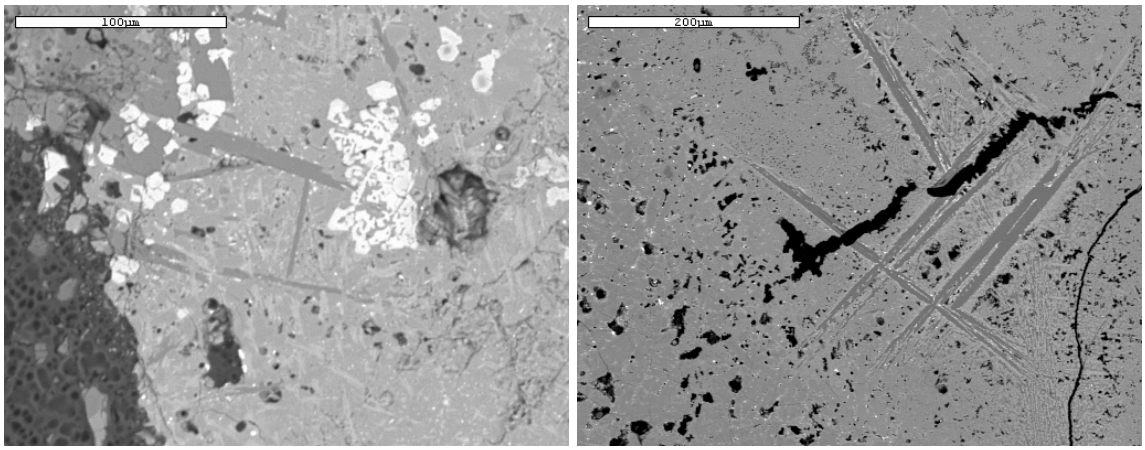

igure 7.6: Left hand image (sample 1T) consists of prominent dark anorthite laths and white hercynite in two toned glass. The right hand image is from sample 1S. The glass is differentiated into grey and light grey phases and very small iron-oxide phases (white).

7.2.8 CCSEM analysis of the hand-picked heated rock fragments

The feed coal contains rock fragments such as siltstone, mudstone, carbonaceous shale and sandstone. It is imperative to determine the role of these stones during coal gasification.

The CCSEM and XRD analyses (Table 4.12 and Table 4.11) of these common rock fragments in the coal feedstock indicate that these stones contain major minerals (kaolinite, quartz, muscovite/illite and microcline) and minor minerals (dolomite, pyrite, calcite, zircon, apatite, rutile and monazite). In most cases, the minor minerals in the coal are associated with these rock fragments taken from the turn-out samples 1T, 8T, 16T and 24T (Figure 7.7). The proportion of kaolinite, quartz, muscovite/illite and microcline in the rock fragments vary significantly.

During the thermal treatment of rock fragments, clays (kaolinite, muscovite/illite) started to lose water of hydration at elevated temperatures ranging from 450-1000°C to form reactive aluminium silicates. It is apparent from images of the heated rock fragments that the "kaolinite" in the heated rock fragment particles hand-picked from sample 1T (which has passed through the gasification temperature zones and exited the gasifier) (Figure 7.7) has distinct desiccation cracks attributed to the dehydration (ash sample 1T, Figure 7.7 and Figure 7.8). Some quartz particles in the heated rock fragments show sign of cracks, but still maintain the physical and chemical properties of quartz in the original coal. Interestingly, the elongated muscovite/illite and angular microcline transformed to form a molten K-bearing glass with Al/Si ratios similar to coal muscovite/illite and microcline (Figure 7.8).

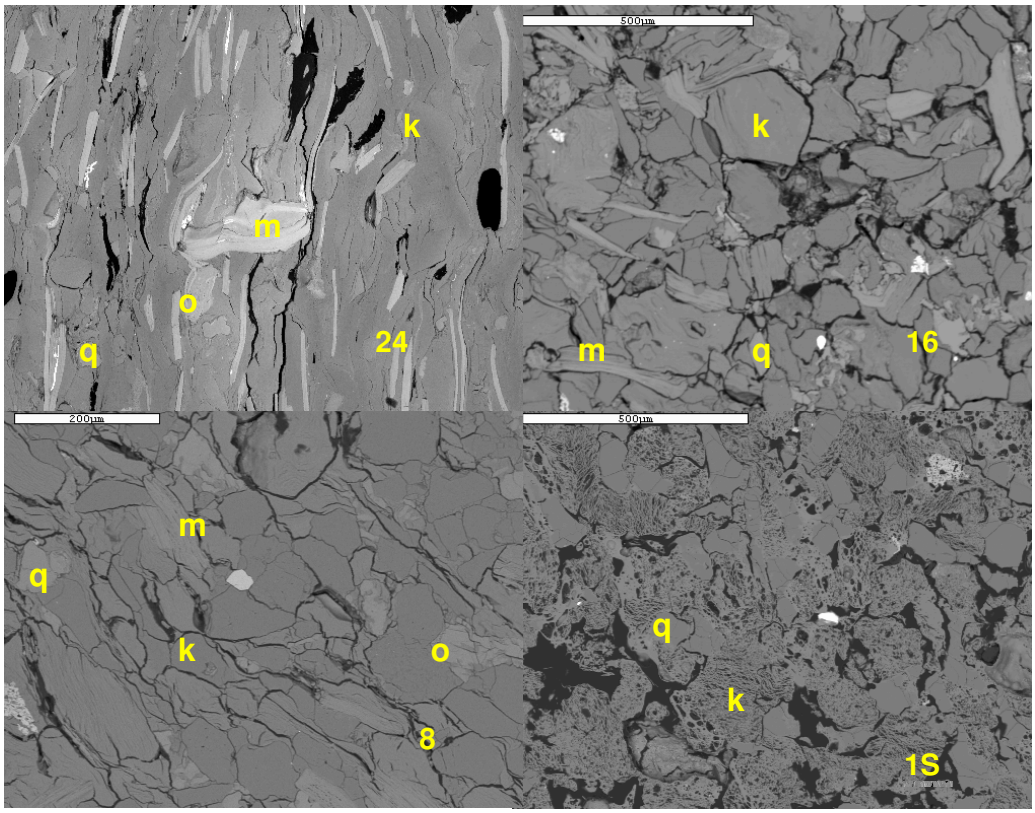

Figure 7.7. Different rock fragments with varying proportions of kaolinite (k), quartz (q), muscovite/illite (m) and microcline (m). Sample numbers (1T (Siltstone), 8T, 16T and 24T) are shown. Scale bar is 200µm.

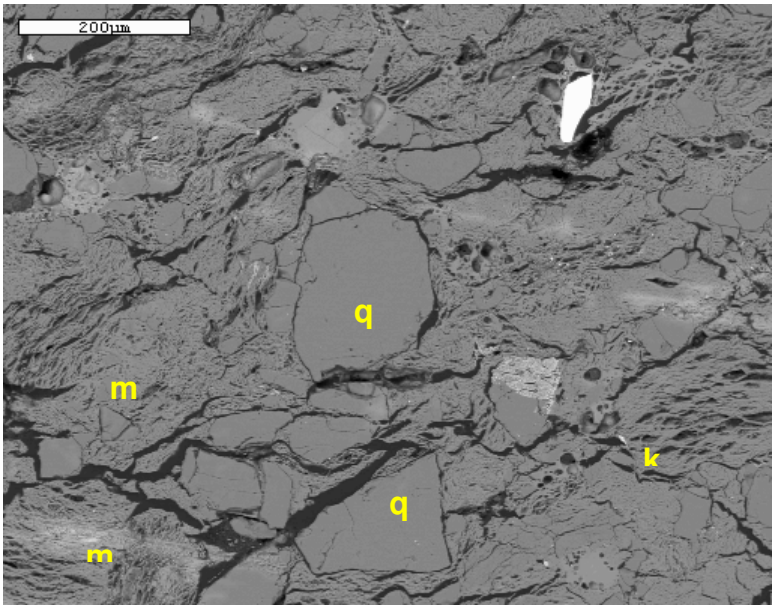

Figure 7.8: Detailed view of rock fragment in sample 1T. Note the dehydrated "kaolinite" (k), angular quartz (q), and molten muscovite/illite (m). Scale bar is 200µm.

It is suggested that significant proportions of mineral matter (non-mineral inorganic elements and minerals) in rock fragments transformed at elevated temperatures in-situ and attached

themselves to the melt to form heterogenous clinkers without chemically participating in the formation of a melt. However, there are some reactive aluminium silicate (metakaolinite) particles and fluxing element-bearing mineral (pyrite) particles in the heated rock fragments that can possibly react with glass to enhance the formation of mullite. There are examples of rock fragments reacting with the glass and perhaps influencing the formation of mullite (Figure 7.9).

CCSEM analysis shows that, on average, particles of the heated rock fragments taken from the coarse ash produced from the gasification process are significantly finer than particles of rock fragments hand-picked from the feed coal. The fragmentation of rock fragments into smaller particles can possibly be attributed to the decomposition of minor carbonate and sulphide minerals, as well as the dehydration of clays in the rock fragment during coal gasification.

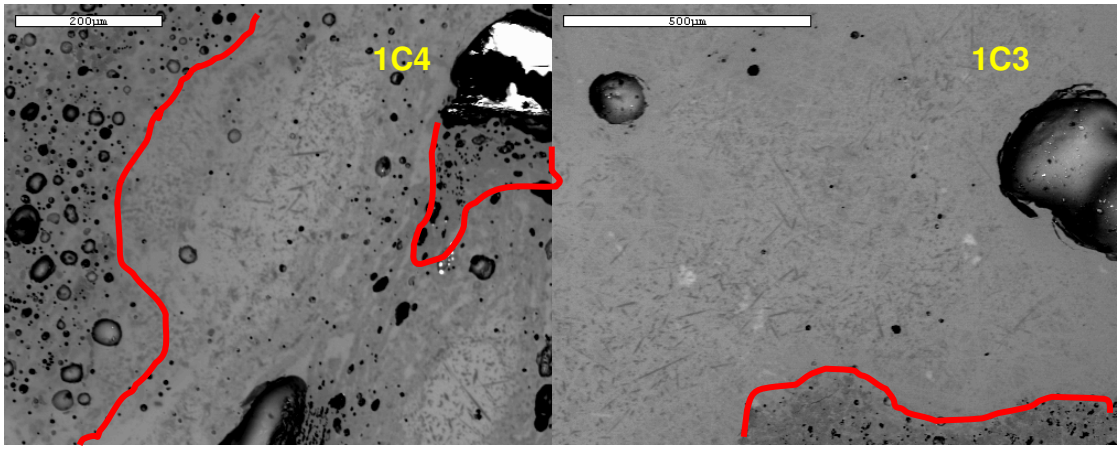

Figure 7.9. Fine dark mullite needles in light grey glass matrix. Not the high proportion of remnant rock fragments associated with mullite.

7.2.9 Transformation of carbonate and pyrite at high temperatures

Heated rock fragment particles that were hand-picked from sample 24T, taken from the turn-out experiment, contain a single large (>10mm) calcite-rich cleat fragment with minor transecting pyrite in filled cleats (Figure 7.10). These extraneous calcite and pyrite-rich cleats in the rock fragment particle transformed partially. The temperature of this rock fragment was below the decomposition temperatures of calcite and pyrite.

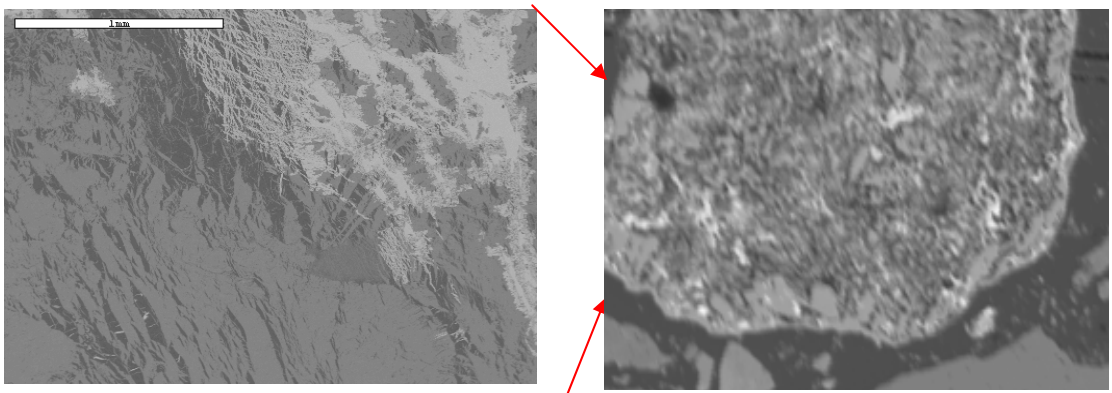

Figure 7.10: Large calcite (Ca) and pyrite rich extraneous cleat fragment. An example of partially transformed calcite/dolomite cleat fragment in the coarse ash is represented on the right hand side. Size of the scale bar is 1mm.

The heated rock fragment particle of sample 8T, shown in Figure 7.11, comprises the Fe-oxide/ Fe-S-oxide/pyrrhotite that are high temperature transformation products of the extraneous pyrite. The spherical light grey grains in the heated rock fragment particle are pyrrhotite, the grey phase is Fe-S-oxide and the dark grey is Fe-oxide. The heated rock fragment particle attached to the particle of clinker consists of anorthite crystals and glass particles. There is no evidence of reaction between the partially oxidised pyrite and dehydrated kaolinite.

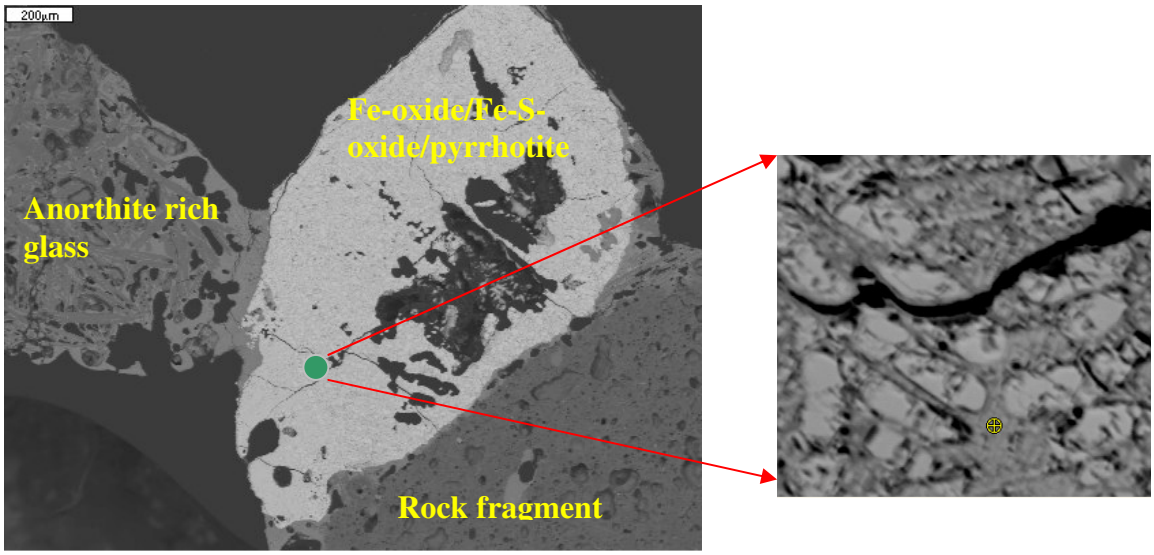

Figure 7.11: Large extraneous "Fe-oxide/Fe-S-oxide/pyrrhotite" particle attached to rock fragment and anorthite rich glass fragment in the coarse ash: scale bar is 200µm). The scale bar of Fe-oxide/ Fe-S-oxide/pyrrhotite is 20um.

In conclusion, the CCSEM results for the heated rock fragments reveal that a significant proportion of minerals in these stones transformed in-situ during gasification. Kaolinite dehydrated at elevated temperatures to form reactive aluminosilicate. Quartz cracked, forming small quartz fragments. The muscovite or illite in the rock fragment transformed at elevated temperatures to K-bearing glass with an Al/Si ratio similar to muscovite/illite or microcline present in the original feed coal. Almost all the extraneous pyrite particles in the coal transformed at elevated temperatures to form iron oxide particles during coal gasification.

7.2.10 Characterisation of the homogenised turn-out samples taken from the gasifier

Figure 7.12 and Appendix C, Table C2 show the concentrations of phases in the turn-out samples taken from the different zones of the gasifier determined by CCSEM. From the results given in Figures 7.12 and 7.13 it is clear that the proportions of phases increase from sample 24T, which was taken before the pyrolysis stage, to sample 1T, which is the gasification ash exiting the gasifier. As expected, the proportion of interstitial and matrix glass has increased from 4.2 mass-% in sample 24T to 30.3 mass-% in sample 1T (Figure 7.12).

It is interesting to note that the proportion of metakaolinite, which is the high temperature transformation product of kaolinite, as well as the proportion of CaO/MgO in the turn-out samples decrease; while glasses of kaolinite (carbonate) increase significantly during coal gasification (Figure 7.13). This supports the suggestion that carbonates (dolomite and calcite), which are associated with kaolinite in the coal, reacted with each other and kaolinite at elevated temperatures and pressures to form a melt resulting in glasses and crystalline phase formation during coal gasification. Interestingly, a low proportion of iron-bearing phases derived from the reaction between kaolinite and pyrite was formed in the turn-out samples (Figure 7.14). From these results it can be concluded that a major proportion of carbonates (dolomite, siderite and calcite) that are associated with kaolinite, lower the ash fusion temperature of kaolinite at elevated temperatures forming a melt; whereas a small proportion of pyrite particles that are associated with kaolinite also contributes to sintering or slagging of mineral matter at elevated temperatures during coal gasification.

There is a marginal decrease in the quartz content. Figures 7.7 and 7.8 show that the quartz grains in the bulk gasification ash, heated stone and clinker samples are typically irregular, broadly equidimensional particles, essentially pure and probably represent unreacted fragments inherited from the coal and non-coal (sandstone, siltstone, carbonaceous shale) components in the feedstock to the gasification process. This implies that quartz, at the existing operating temperatures of the gasification process, does not participate in the chemical reactions.

Extensive CCSEM investigations of gasifier ash have shown that muscovite and orthoclase in rock fragments alter in-situ and do not necessarily participate in glass formation (Matjie et al., 2006). This is confirmed by the consistent proportion of orthoclase and muscovite glass.

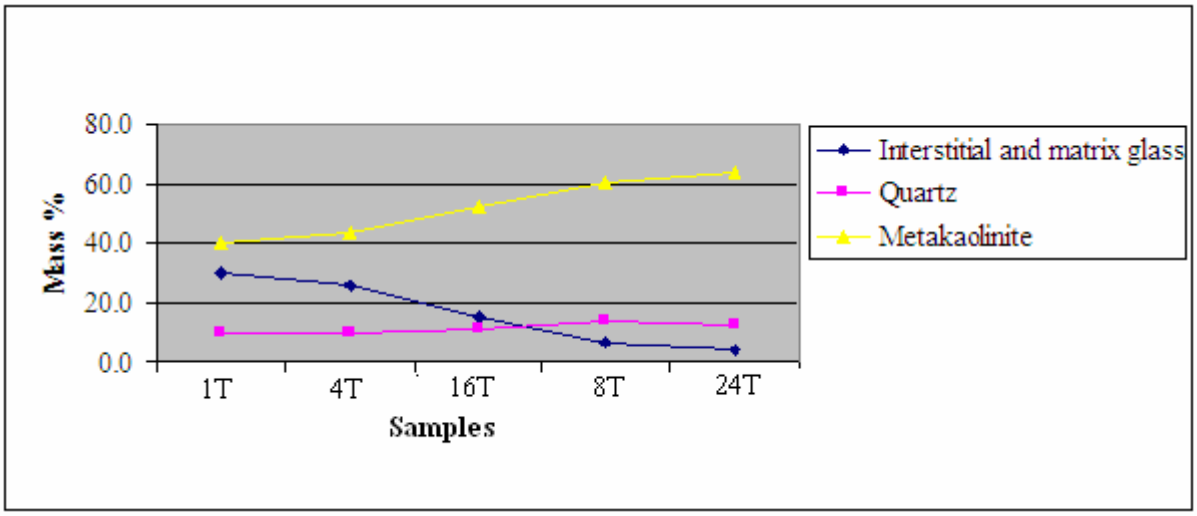

Figure 7.12: Proportions of glass, quartz and metakaolinite.

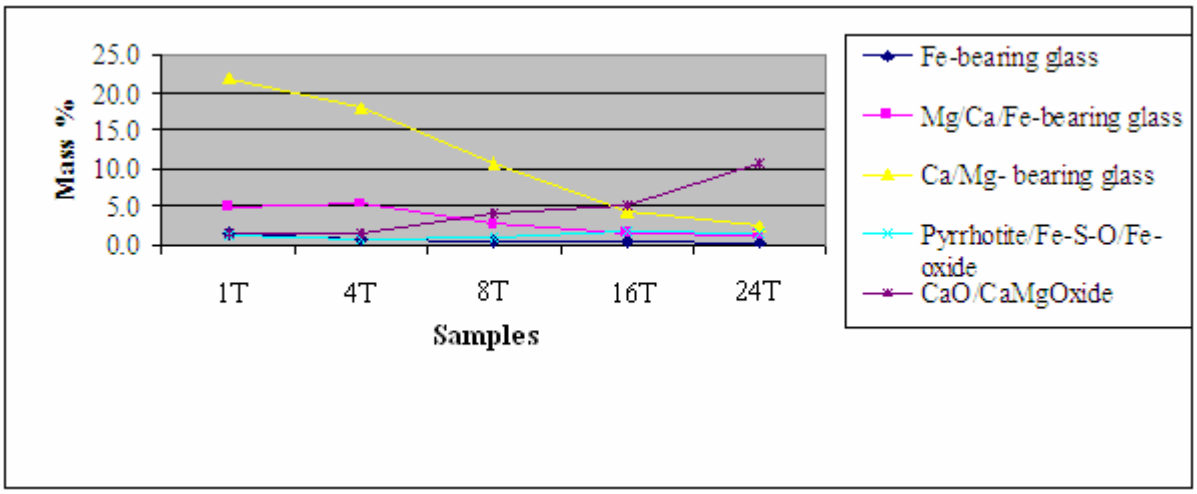

Figure 7.13: Proportions of silicates and metal oxides in the turn-out samples.

Based on the CCSEM results for the turn-out samples, it is clearly that carbonates (dolomite or ankerite, siderite and calcite) that are associated with kaolinite, lower the ash fusion temperature of kaolinite at elevated temperatures, forming a melt. Anorthite and mullite crystallised out from the melt, resulting in formation of different glasses. Interestingly, a low proportion of iron-bearing phases derived from the reaction between kaolinite and pyrite was formed in the turn-out samples. This could imply that some extraneous pyrite and pyrite particles associated with carbon matrix, contribute little to sintering or slagging of mineral matter at elevated temperatures during coal gasification. The hypothesis (the included minerals are accountable for clinker formation in the gasifier) was successfully tested in this study.

7.2.11 SEM-EDS analysis of the hand-picked clinkers and heated rock fragments from the selected dig-out samples

The back-scattered electron images (Figures 7.14 and 7.15) of the clinker particles, taken from sample 7D during the dig-out test, indicate that these ash particles (formed at elevated temperatures in the gasifier) contained two high temperature transformation phases (anorthite and mullite). This implies that high temperature transformation products of the included dolomite and calcite minerals that were associated with kaolinite reacted with the reactive high temperature transformation product (meta-kaolinite) of kaolinite at elevated temperatures to form a melt. On cooling the melt with steam, anorthite and mullite crystallise out from the melt resulting in the formation of glasses containing a different chemical composition. The electron microprobe and CCSEM results for the turn-out ash particles corroborated reports in this study.

The heated rock fragments containing some devolatilised kaolinite particles, partially transformed quartz, unaltered quartz grains and potassium feldspar being present in the gasifier attached to the cooling melt during crystallisation of anorthite and mullite to form clinkers (Figures 7.14 and 7.15). The presence of the mullite and anorthite crystals in the heated rock fragments implies that some fluxing elements-bearing minerals, including calcite and dolomite present in the stone, reacted with kaolinite at elevated temperatures to form an in-situ melt of the heated rock fragments (Figure 7.15).

Although iron as ferrous (Fe^{2+}) from pyrite reduces the ash fusion temperature of mineral matter in coal during thermal treatment, the majority of iron from the extraneous pyrite particles contributes little to the sintering and slagging of mineral matter during coal gasification. The CCSEM and SEM-EDS results (Figures 7.10, 7.11 and 7.14) for ash samples treated in this study, confirmed that some extraneous pyrite particles transformed at elevated temperatures to pyrrhotite and hematite, without reacting with the high temperature transformation products of kaolinite to form a melt. Some of the iron species may react with the available metal oxide to form spinel such as hercynite ($FeAl_2O_4$), ferrianspinel ((Fe, Mg)Al_2O_4) phases, or magnesioferrite ($MgFe_2O_4$) (Figure 7.14, Figure 7.6). Other iron particles from trace amounts of siderite, iron from ankerite and iron from the kaolinite and pyrite association in the coal can contribute significantly to the sintering and slagging of mineral matter during coal-conversion processes.

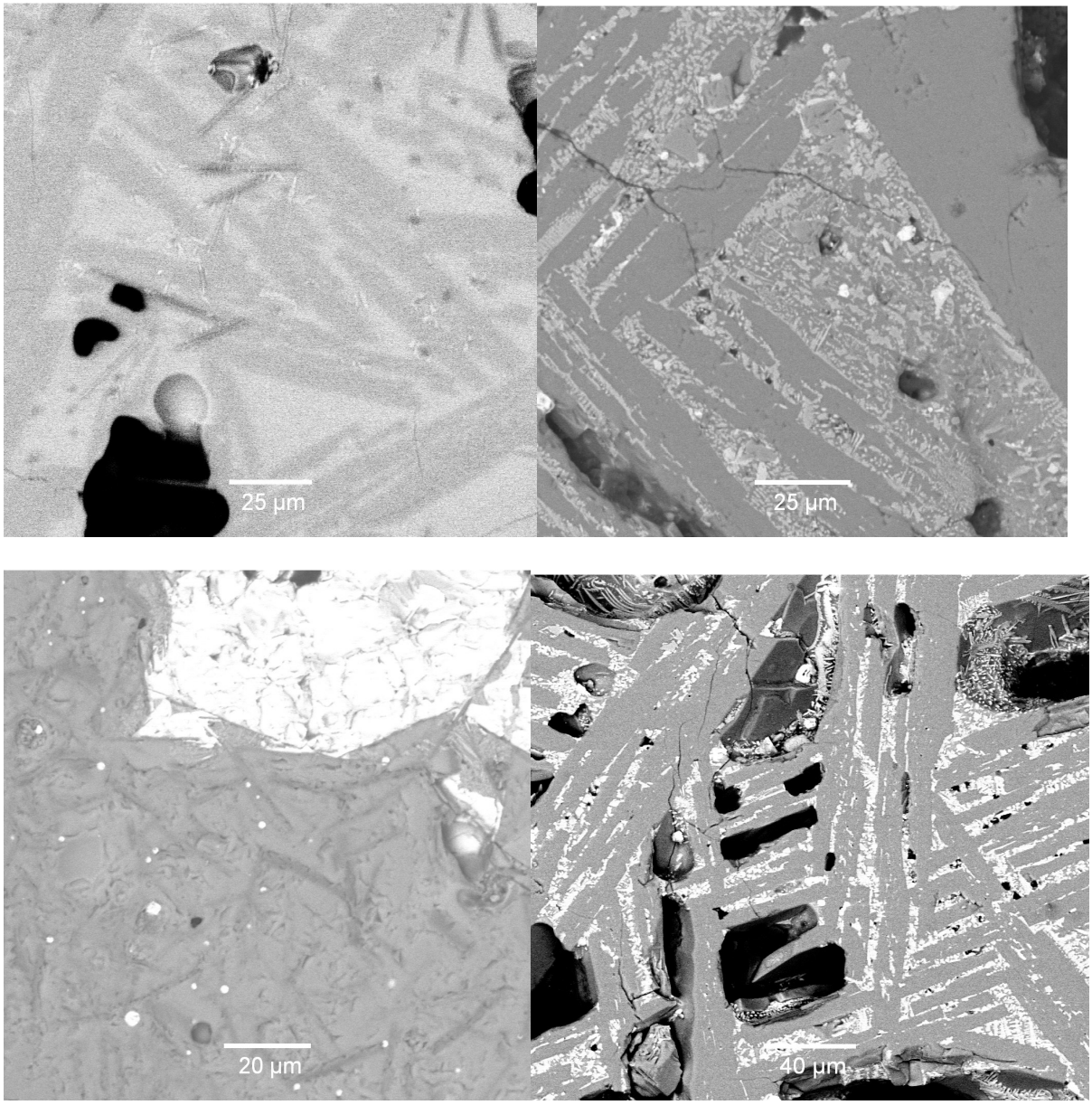

Figure 7.14: Back-scattered images of dig-out clinkers 6D and 7D: the left top image of clinker 7D: shows anorthite and mullite (dark) needles crystals and right top image shows anorthite crystals (dark grey). Scale bar for the top images is 25µm. The bottom images of clinkers 7D and 6D show mullite and anorthite crystals. The left bottom image of clinker 7D shows white dots of iron oxide. Scale bar for the left bottom image is 20µm and for the second bottom image is 40µm.

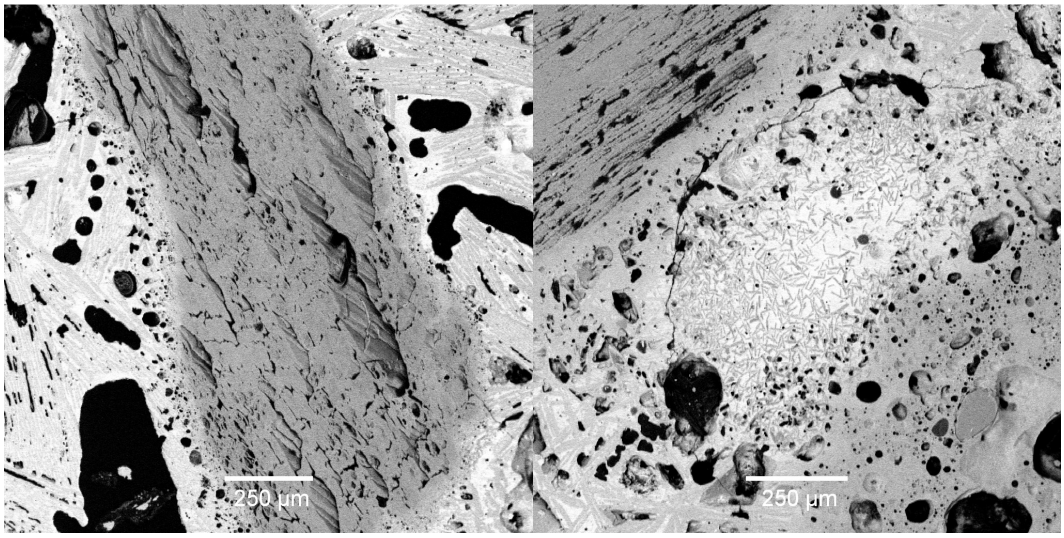

Figure 7.15: First BSE image of the heated stone 6.7D shows devolatilised kaolinite; and the second image (right) of heated stone 6.11D shows heated carbonaceous shale attached to anorthite and mullite crystals in the heated stone. Scale bar for the images is 250µm.

7.2.12 Determination of glass and mineral compositions in the gasification ash particles by electron microprobe analysis

Electron microprobe analysis was used to determine the chemical composition of the principal crystalline and glassy phases in polished sections and polished thin sections of selected lump clinker samples. Images illustrating the textures in a typical sample, showing the modes of occurrence of quartz, feldspar and glassy phases, are provided in Figure 7.16. The chemical composition of the quartz, feldspar and aluminosilicate glass for a wider range of samples, based on the microprobe study, is given in Table 7.6.

- **Quartz and feldspar crystals**

The quartz grains in the bulk gasification ash, heated stone and clinker samples are typically irregular, broadly equidimensional particles, probably representing unreacted fragments inherited from the coal and non-coal (sandstone, siltstone, carbonaceous shale) components in the feedstock to the gasification process. Figure 7.16a, for example, shows a series of silt-sized quartz grains each around 10µm in size. Table 7.6 indicates that the quartz particles are essentially pure, with usually more than 98% SiO_2. Traces of Al_2O_3, Fe_2O_3, CaO and TiO_2 are also present in some cases.

Although both potassium feldspar and anorthite (Ca feldspar) were noted in the bulk coal gasification ash sample (Table 7.6), the feldspar crystals in the other heated stone and clinker samples were found to be essentially pure anorthite. As indicated in Table 7.6, most of the feldspars analysed have chemical compositions close to that of stoichiometric anorthite, which is 44.3% SiO_2, 35.6% Al_2O_3 and 20.1% CaO. A small concentration (up to around 0.5%) of Na_2O is also indicated in some cases, occurring in solid solution. Measurable concentrations of Fe_2O_3, MgO and TiO_2 reported in some samples may represent inclusions within the feldspar crystals.

Potassium feldspar, in the form of microcline, is commonly present in the non-coal rocks associated with South African coal seams (Pinetown et al., 2006). The potassium feldspar noted in the bulk coal gasification ash (Table 7.6) may thus represent residual particles originally of detrital origin. The euhedral shape of the anorthite crystals (Figure 7.16B), however, and their textural relationship to the associated glassy matrix, suggest that most of the anorthite crystals are formed in the gasification ash from the molten state, in a manner analogous to the crystallisation of igneous rocks from magmatic materials. The textural features suggest that melting and subsequent crystallisation has taken place and that solid-state reactions resulting in feldspar formation, identified in combustion-based studies (Benson, 1987; French et al., 2001; Jung, 1996; Reifenstein, 1999), are less significant in the fixed-bed gasification process.

- **Aluminosilicate glass**

The aluminosilicate glass in the coal gasification ash and clinker samples, as determined by electron microprobe analysis (Table 7.6), varies considerably among the samples studied. Based on averages for a number of individual points, the proportion of SiO_2 in the glass ranges from around 20% to around 70% and Al_2O_3 from 15 to 35%. Although one or two samples have higher values, the proportion of Fe_2O_3 in the glass is mostly less than 10% and CaO mostly less than 5%. MgO, TiO_2 and K_2O are also significant components of the glass in a number of the samples studied.

Table 7.6: Composition of main mineral fragments and glass matrix in coal gasification ash samples (wt %), as determined by electron microprobe analysis

	Pts	SiO_2	TiO_2	Al_2O_3	Fe_2O_3	MgO	MnO	CaO	Na_2O	K_2O	P_2O_5	SO_3	Total
Quartz													
Bulk gasification ash	7	98.98	0.01	0.29	0.20	0.01	0.01	0.01	0.02	0.15	0.01	0.02	99.71
Clinker 1	2	100.43	0.02	0.04	0.01	0.00	0.01	0.00	0.00	0.00	0.02	0.01	100.53
Clinker 2	4	99.73	0.05	0.07	0.02	0.00	0.01	0.01	0.01	0.01	0.01	0.01	99.93
Clinker 7	8	98.39	0.09	0.14	0.03	0.01	0.02	0.01	0.01	0.01	0.02	0.02	98.75
Clinker 9	5	94.37	0.63	3.19	0.19	0.09	0.00	0.20	0.06	0.08	0.11	0.01	98.93
Clinker 10	3	99.20	0.02	0.04	0.04	0.00	0.01	0.02	0.00	0.01	0.04	0.01	99.38
Heated stone 3	4	100.16	0.02	0.02	0.11	0.00	0.01	0.02	0.01	0.02	0.00	0.01	100.38
Feldspar K-feldspar													
Bulk gasification ash	1	63.73	0.04	18.41	0.11	0.01	0.00	0.00	0.41	16.13	0.00	0.01	98.86
Anorthite													
Bulk gasification ash	1	42.42	0.09	33.87	0.10	0.12	0.03	20.60	0.02	0.04	0.13	0.09	97.51
Clinker 1	7	43.74	0.16	34.40	0.38	0.38	0.03	18.48	0.36	0.08	0.10	0.01	98.12
Clinker 2	7	44.22	0.11	34.41	0.37	0.25	0.01	18.20	0.54	0.13	0.07	0.02	98.32
Clinker 7	4	43.17	1.28	27.84	2.94	4.16	0.06	16.50	0.47	0.44	0.79	0.09	97.74
Clinker 8	7	44.56	0.29	32.27	1.22	0.99	0.01	17.81	0.76	0.29	0.23	0.04	98.46
Clinker 9	30	45.19	0.36	31.32	1.03	1.17	0.02	16.73	0.76	0.25	0.25	0.04	97.12
Clinker 10	7	44.37	0.14	34.13	0.40	0.25	0.02	17.85	0.49	0.14	0.09	0.02	97.91
Si-Al glass													
Bulk gasification ash	14	58.37	0.42	20.90	9.41	0.43	0.02	4.80	0.16	2.86	0.03	0.16	97.55
Clinker 1	20	44.60	2.75	14.21	4.22	13.02	0.26	13.09	0.43	1.72	1.48	0.12	95.89
Clinker 2	20	47.92	1.46	33.45	3.97	3.87	0.04	3.77	0.38	1.45	1.49	0.04	97.85
Clinker 7	20	70.18	2.94	21.01	0.82	0.47	0.02	0.47	0.28	1.30	0.04	0.02	97.55
Clinker 8	35	22.23	2.37	33.73	16.88	18.08	0.14	4.86	0.13	0.09	0.55	0.02	99.10
Clinker 9	8	58.45	2.20	21.72	1.39	2.48	0.03	4.07	0.23	0.64	0.52	0.07	91.80
Clinker 10	16	56.56	1.13	28.70	2.61	1.43	0.05	2.77	0.39	1.61	0.49	0.11	95.84
Heated stone 3	54	54.83	0.24	15.80	1.74	2.11	0.01	3.12	3.46	0.98	0.06	1.38	83.72

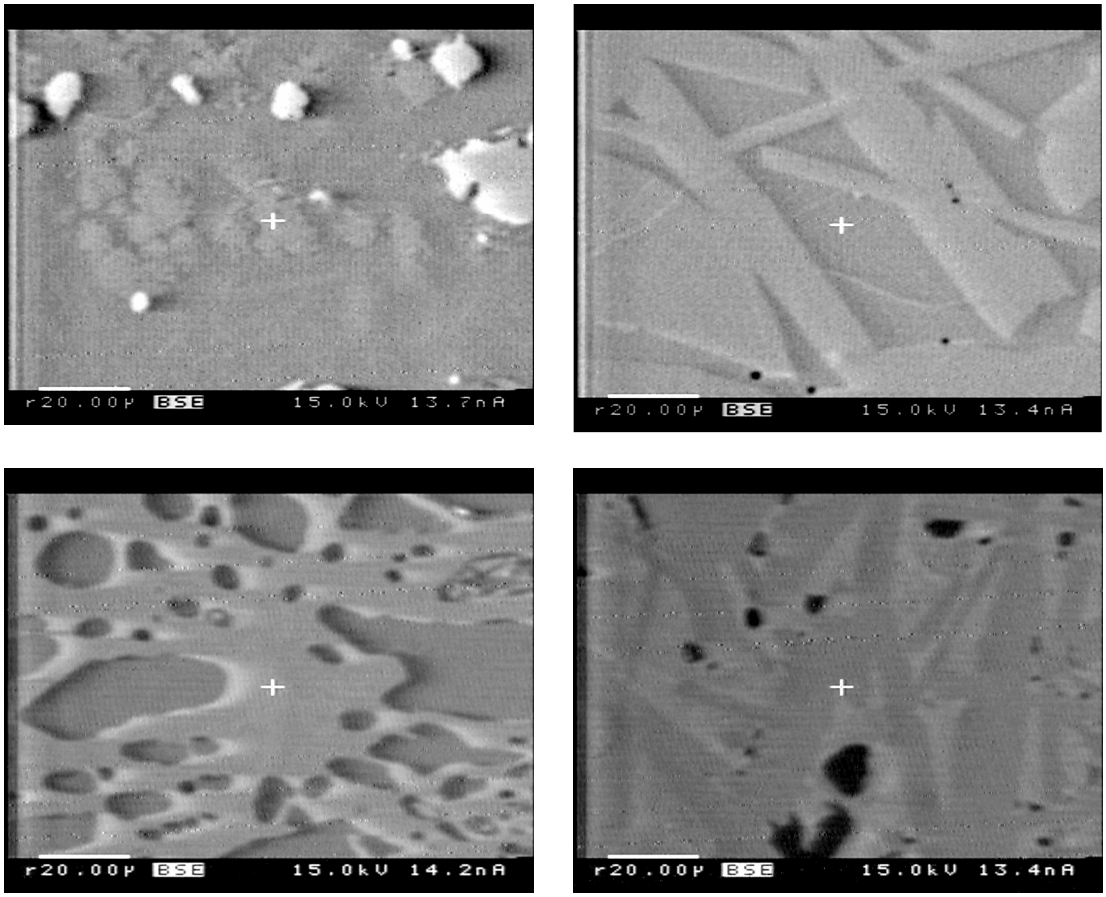

Figure 7.16: Electron microprobe images of slag samples (back-scattered electron mode) in Clinker 2. Top left: quartz particles (mid grey) set in glassy matrix; top right: elongate anorthite crystals (light grey) with interstitial glass; bottom left: homogeneous vesicular glass; bottom right: anorthite crystals (mid grey) with vesicles (black) in interstitial light grey glass. Scale bar in each case represents 20µm.

Figure 7.17 indicates the correlation between the proportions of the main oxides in the aluminosilicate glass for each sample, based on averaging a number of points as indicated in Table 7.6 and the proportions of the same oxides, inferred from the bulk chemistry of each sample and the quantitative XRD data (Table 7.5). Although there is considerable scatter, the overall trend for SiO_2, Fe_2O_3 and CaO suggests a positive correlation, with many of the individual points falling close to the diagonal representing equality for the two different types of evaluations. However, the overall trend for Al_2O_3 seems to be almost the opposite, with a negative correlation; notwithstanding this apparent trend, over half of the points still fall close to the equality line.

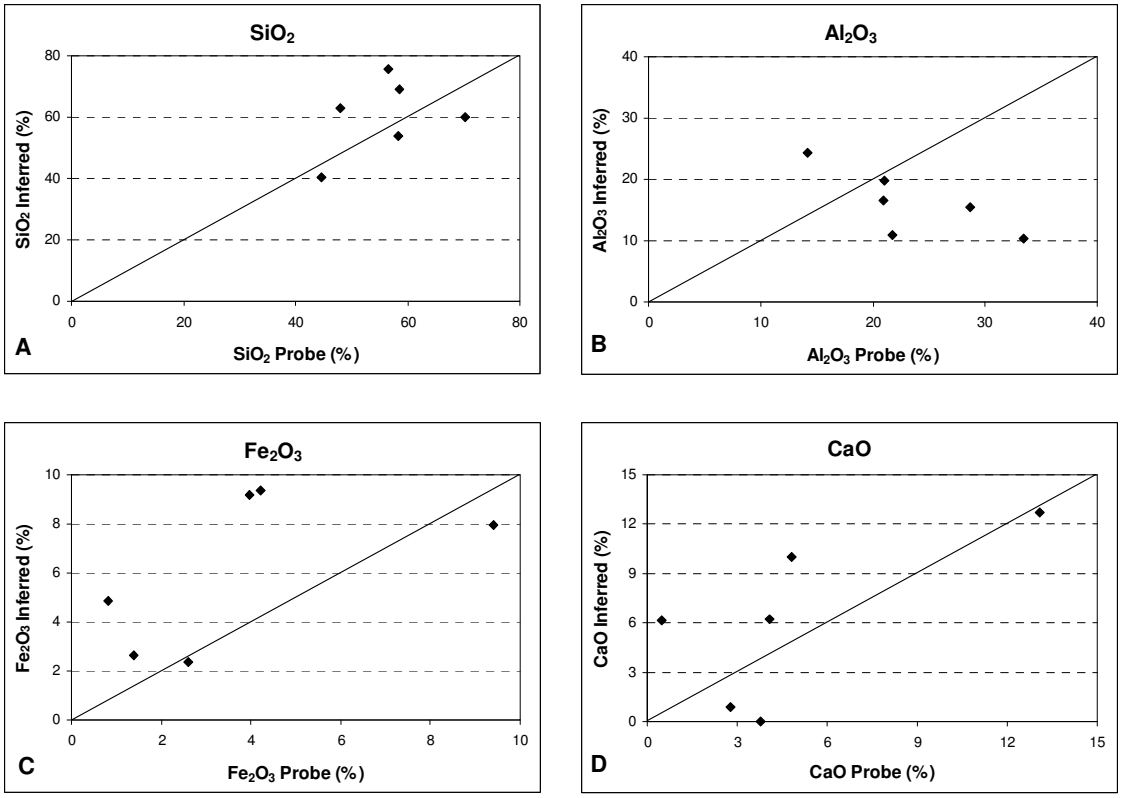

Figure 7.17: Correlation between key oxide percentages in aluminosilicate glass as determined by electron microprobe analysis (Table 7.6) and inferred percentages of same oxides in glass fraction interpreted from bulk composition and XRD analysis (Tables 7.4 and 7.5). A: SiO_2; B: Al_2O_3; C: Fe_2O_3; D: CaO.

- **Other particles and phases**

A range of other particles and glassy phases is also present in the samples; the composition of some of these is indicated in Table 7.7. They include particles identified as corundum (with almost 100% Al_2O_3) and particles (probably representing rutile or anatase) that consist almost entirely of TiO_2. Small proportions of SiO_2 and/or Al_2O_3 in some particles may represent inclusion of glass or other phases in the analysed field. Other phases, with roughly equal proportions of SiO_2 and Al_2O_3 have been tentatively identified as metakaolin, probably derived from kaolinite in the feed coal. Although mullite is identified in the various materials by XRD, the lack of contrast between this mineral and the associated aluminosilicate glass makes it difficult to identify and analyse the mullite composition separately by microprobe techniques. The individual mullite crystals are also likely to be sub-micron in size, so that the spot size embraced in any microprobe analysis would inherently include at least some of the associated glassy matrix as well.

An alumino-phosphate phase is also indicated by the microprobe data. Although departing from the stoichiometric composition of crandallite (13.6% CaO, 37.1% Al_2O_3, 34.0% P_2O_5, 15.3% H_2O), this material probably represents a product of the gorceixite-group material identified in the LTA of the feed coal (Table 4.11).

A range of phases rich in iron and magnesium are also indicated in Table 7.7. Some of these may represent discrete hercynite ($FeAl_2O_4$) or ferrianspinel ($(Fe,Mg)Al_2O_4$) phases, while others, such as in sample clinker 10, represent Fe-Mg silicate components, apparently occurring in a more glassy form. The Fe-Mg silicate minerals in the clinkers analysed in this study may have been derived from reactions between fluxing elements-bearing minerals (pyrite, calcite, and dolomite) and kaolinite or illite at elevated temperatures during coal gasification.

Phases consisting of iron and sulphur are also present, with a composition close to that of pyrrhotite (FeS, 63.6% Fe, 36.3% S) rather than pyrite (FeS_2, 46.6% Fe, 53.4% S). These are probably reaction products of pyrite in the original feed coal.

In conclusion, the bulk gasification ash, heated stone and clinker samples produced by the gasification process contain fragments of heat-altered rock materials, set in an often vesicular, partly crystalline glassy matrix. Quartz and possibly K-feldspar in the feed coal or admixed non-coal rocks may pass unaltered into the bulk gasification ash, along perhaps with titanium or iron-titanium oxides and aluminophosphate minerals. Extraneous pyrite particles also react to form pyrrhotite as part of the gasification process. Although products of solid-state reactions may be preserved in some of the heat-altered fragments, anorthite that has crystallised from molten aluminosilicate material is contained within a glassy matrix in a manner analogous to the formation of igneous rocks.

In the next chapter, the FactSage results for the selected clinker and heated rock fragment particles obtained, after using the area SEM-EDS analysis of these particles, are discussed.

Table 7.7: Composition of other coal gasification ash components (wt %) as determined by electron microprobe

	Pts	SiO_2	TiO_2	Al_2O_3	Fe_2O_3	MgO	MnO	CaO	Na_2O	K_2O	P_2O_5	SO_3	Total
Corundum													
Clinker 8	2	0.03	0.00	99.02	0.19	0.00	0.01	0.07	0.00	0.00	0.00	0.03	99.36
Metakaolin													
Clinker 8	5	49.57	0.50	42.08	0.87	0.17	0.00	0.11	0.34	0.35	0.08	0.06	94.13
Ti-oxide													
Clinker 7	2	2.84	93.33	0.77	0.19	0.02	0.01	0.07	0.02	0.08	0.02	0.01	97.37
Clinker 10	3	11.61	82.81	4.23	0.62	0.15	0.02	0.14	0.14	0.69	0.08	0.03	100.50
Heated stone 3	1	0.19	98.21	0.19	0.17	0.00	0.00	0.00	0.01	0.03	0.00	0.00	98.78
Al-phosphate													
Clinker 9	6	3.89	0.13	24.18	0.52	1.75	0.02	26.13	0.45	2.41	27.39	0.01	86.88
Fe Mg-rich													
Clinker 2	1	13.05	13.66	6.10	59.27	3.84	0.44	1.85	0.26	1.07	1.33	0.29	101.14
Clinker 8	5	0.38	47.45	0.27	49.45	2.05	0.75	0.59	0.02	0.10	0.04	0.17	101.27
Clinker 9	2	1.01	1.06	23.09	68.05	8.01	0.07	0.11	0.01	0.03	0.05	0.00	101.49
Clinker 10	9	40.23	3.60	10.00	23.33	15.06	0.30	4.77	0.27	0.75	2.08	0.28	100.66